

## Synthesis and NMR Spectroscopic Study of the Self-Aggregation of 2-Substituted Benzene-1,3,5-tricarboxamides

Christian Invernizzi,<sup>[a]</sup> Claudio Dalvit,<sup>[b]</sup> Helen Stoeckli-Evans,<sup>[c]</sup> and Reinhard Neier\*<sup>[a]</sup>

**Keywords:** Supramolecular chemistry / Self-assembly / Hydrogen bonds / Pi interactions / Liquid crystals

The self-assembly of *N,N',N''*-trialkylbenzene-1,3,5-tricarboxamides (BTAs) **1** or of "crowded" BTAs **11** and **12** lead to supramolecular columnar-stacked structures with attractive material properties. The introduction of three alkoxy groups is reported to reinforce the self-assembly process. The influence of a single substituent introduced onto the aromatic

core of BTA significantly affects the self-assembly process. The aggregation process of 2-substituted BTAs in the bulk and in solution, as studied by DSC, POM, X-ray diffraction and <sup>1</sup>H NMR experiments, is impaired by hydrogen-bond-accepting substituents but strengthened by non-hydrogen-bond-accepting substituents.

### Introduction

Understanding the processes that create order from simple building blocks is the key to deepening our insight into the life and material sciences.<sup>[1]</sup> Data identifying and quantifying interactions in solution and correlating them with material properties help to overcome the gap between models based on the interplay between individual molecules and material properties. The relatively small number of widely known interactions responsible for self-assembly are combined with a wealth of empirical data. "Our ability to predict the structural features and the functional outcome of the assembled materials is still limited and most of the learning is done in retrospect".<sup>[2]</sup> *N,N',N''*-Trialkylbenzene-1,3,5-tricarboxamides (BTAs) **1** form supramolecular columnar-stacked structures<sup>[3]</sup> that show attractive material properties.<sup>[4]</sup> The observation of discotic mesophases based on the triamide structures has been attributed to the occurrence of  $\pi$  stacking<sup>[5]</sup> and to the simultaneous formation of the maximum number of hydrogen bonds.<sup>[3,6]</sup> The hypotheses used for rationalizing the material properties of BTAs are based on X-ray structures of simpler crystalline models and on modelling studies (see parts a,b of Figure 4 and Supporting Information).<sup>[7]</sup>

The unexpected results obtained in the context of our approach to creating novel addressable organic electronic elements<sup>[9]</sup> induced us to undertake studies correlating material properties with NMR experiments. The starting point

of our studies was a simple design exploring linear dimers with minimal disturbance of the benzenetricarboxamide basic structure. The physical properties of interest in such mesomorphic materials, such as 1D charge transport, strongly depend on the molecular alignment in the liquid crystalline phases.<sup>[10]</sup> Enhanced control over self-organization of discotic compounds is expected by covalently linking two discotic units through a rigid linker.<sup>[9b,11]</sup> This approach aims to create an interface between materials by using nano-sized structures and microtechnology. Predicting reliably the efficiency of the self-assembly process and as a consequence the material properties is still the biggest challenge.

The first synthesis of BTAs was achieved by Curtius in 1915.<sup>[12]</sup> In their pioneering work published in 1988, Matsunaga et al. reported the first controlled fabrication of columnar liquid crystals based on BTA as a fundamental unit (Figure 1, a).<sup>[3]</sup> The discovery of the liquid crystalline behaviour of **1** stimulated intense studies of BTA derivatives. Detailed studies by Meijer and co-workers elucidated the cooperative nature of the supramolecular assembly.<sup>[13]</sup> The nucleation constant  $K_n$  and the elongation constant  $K_e$  of the cooperative aggregation process of the *N,N',N''*-trioctylbenzene-1,3,5-tricarboxamide derivative were determined by these authors.<sup>[13b]</sup> An impressive number of modifications of BTAs have been reported, varying the lateral chains, introducing stereogenic centres into the chains,<sup>[14]</sup> changing the polarity<sup>[6]</sup> and adding gallic acid elements to impose additional  $\pi$  stacking.<sup>[15]</sup> Nuckolls and co-workers reported in 2001 the first modification of the central aromatic core. The 2,4,6-trialkoxy-substituted BTA **11**, referred to as a "crowded arene", was described as a new substance forming mesomorphic materials (Figure 1, b).<sup>[8a,16]</sup> The introduction of dodecyloxy chains into the 2-, 4- and 6-positions in **11** led to considerably stronger intermolecular hydrogen bonds. Nuckolls and co-workers postulated that

[a] Institut de chimie, Université de Neuchâtel, Avenue Bellevaux 51, 2000 Neuchâtel, Switzerland  
E-mail: Reinhard.Neier@unine.ch  
<http://www2.unine.ch/cho/page-7961.html>

[b] NPAC, Université de Neuchâtel, Avenue Bellevaux 51, 2000 Neuchâtel, Switzerland

[c] Institut de physique, Université de Neuchâtel, Avenue Bellevaux 51, 2000 Neuchâtel, Switzerland

Supporting information for this article is available on the WWW under <http://dx.doi.org/10.1002/ejoc.201500506>.

the three additional substituents induced a conformational twist out of planarity. The formation of a columnar superstructure of crowded arenes by replacing the dodecyloxy chains by phenylacetylene substituents has been reported for compound **12** (Figure 1, b).<sup>[8b,17]</sup>

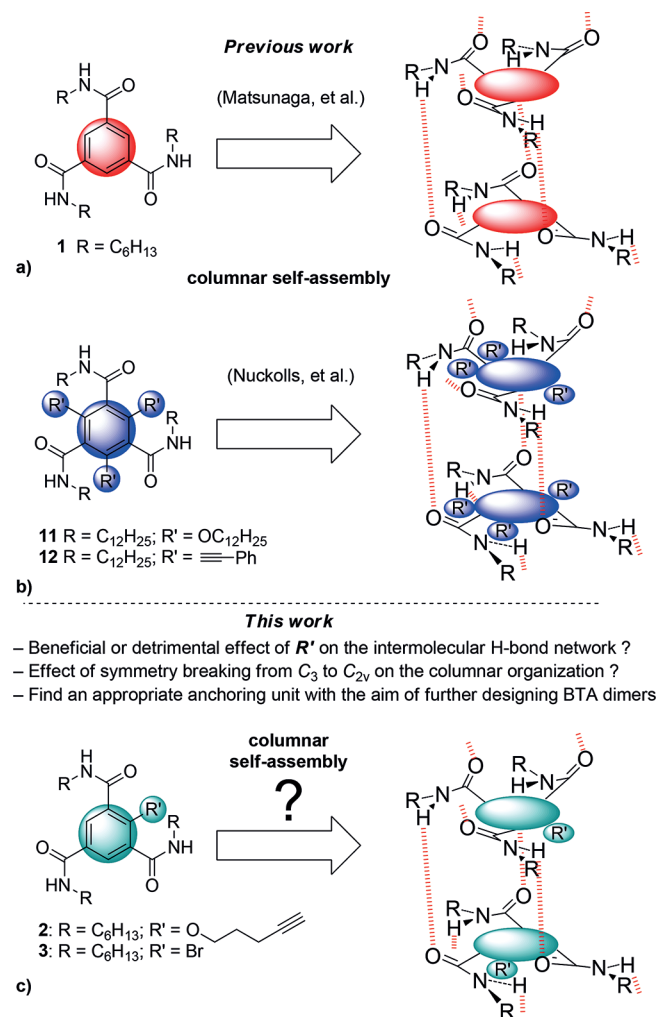


Figure 1. a) Supramolecular architectures of columnar-stacked tri-alkylbenzene-1,3,5-tricarboxamide units **1** reported by Matsunaga et al.<sup>[3]</sup> b) Supramolecular motif of “crowded arenes” 2,4,6-trisubstituted benzene-1,3,5-tricarboxamides **11** and **12** proposed by Nuckolls and co-workers.<sup>[8]</sup> The introduction of three additional substituents on the BTA skeleton strengthened the intermolecular interactions and leads to a wider temperature range for the occurrence of the liquid crystalline phase. c) Tentatively proposed supramolecular structures of columnar-stacked BTA derivatives substituted in the 2-position. To apply the new BTA derived design we had to explore the supramolecular assembly, the molecular properties of the novel structures and the influence of the introduction of a single, disturbing substituent into the skeleton. In parts a–c, the red dashed lines indicate intermolecular hydrogen bonds.

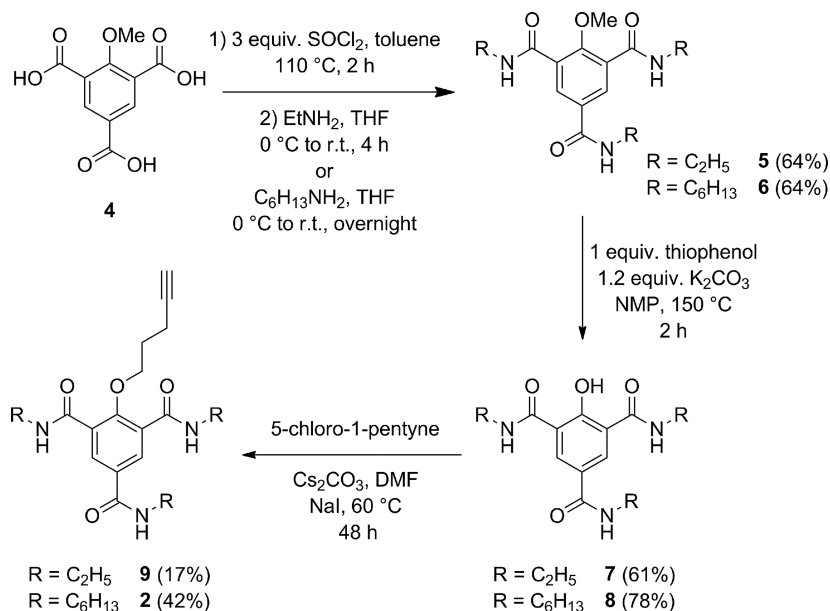
We proposed to introduce a single alkoxy group into the aromatic scaffold to make a “minimal” structural change (Figure 1, c). The alkoxy group would be used as a linker to create covalent linear dimers. To the best of our knowledge, no studies of 2-monosubstituted BTAs have been reported and we have characterized the mechanism of the self-aggregation and the structures of the aggregates of the

novel modified BTAs. We decided to study the assembly of the two BTA derivatives **2** and **3**. We present their synthesis (Scheme 1 and Scheme 2) and the analyses of their supramolecular assembly in the liquid-crystalline and solid states (see the Supporting Information). To elucidate the aggregation mechanism of **2** and **3**, thermodynamic data in conjunction with structural information were extracted by recording their <sup>1</sup>H NMR spectra in solution.<sup>[18]</sup> The two phenomena invoked, hydrogen bonding and π stacking, should be easy to detect by <sup>1</sup>H NMR spectroscopy. The formation of intermolecular hydrogen bonds induces a downfield shift of the amide protons, whereas π stacking causes an upfield shift of the aromatic protons.<sup>[19]</sup> NMR diffusion-ordered spectroscopy (DOSY)<sup>[20]</sup> measures the changes in the diffusion coefficient and allows evaluation of the formation and size of supramolecular aggregates,<sup>[21]</sup> dendrimers<sup>[22]</sup> and proteins.<sup>[23]</sup> The thermodynamic data, derived from concentration-induced variations in the chemical shifts in <sup>1</sup>H NMR experiments, give a readout of the sum of all the forces in place during the aggregation process. The 2-substituted BTA scaffolds in **2** and **3** are compared with the C<sub>3</sub>-symmetric BTA **1**. A comparison of the relative capacities of these molecules to form intramolecular hydrogen bonds provides a measure of the influence of the alkyloxy group in **2** and of the sterically demanding bromine atom in **3** on the aggregation process.

## Results and Discussion

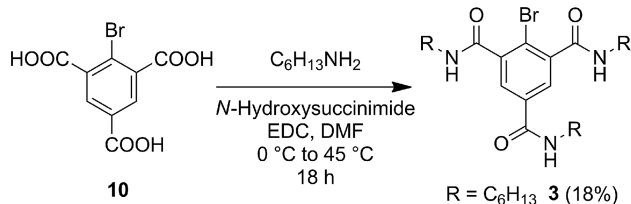
The choice of the introduction of an alkyloxy group was driven by the attractiveness of forming dimeric structures by “click chemistry”. Terminal triple bonds can be selectively and efficiently transformed with the help of Cu-catalysed azido-alkyne “click-chemistry” (CuAAC),<sup>[24]</sup> a strategy that has already been used by our group to form mesogenic dimeric structures.<sup>[9b]</sup> The alkyloxy substituent can easily be introduced by phenol alkylation and varying the alkyne derivative allows modulation of the length of the linker. The study of the material and self-assembly properties of 2-bromo-substituted BTA **3** was envisaged for comparison reasons with a sterically demanding but non-hydrogen-bonding substituent. The synthesis of the 2-alkyloxy-BTA scaffold was started from the previously reported 2-methoxytrimesic acid (**4**; Scheme 1). Compound **4** was prepared according to the procedure reported by Raymond and co-workers.<sup>[25]</sup> A permanganate-mediated oxidation under basic conditions of 2,6-bis(hydroxymethyl)-*p*-cresol furnished the 2-methoxy-triacid **4** in yields comparable to those reported in the literature. The triacid **4** was converted into the corresponding triacyl chloride by employing 3 equivalents of thionyl chloride, which was then treated with an excess of primary amine. The corresponding amides **5** and **6** were isolated in good yields over two steps.

The 2-methoxy-benzamides **5** and **6** were deprotected by nucleophilic methyl ether cleavage according to the conditions reported by Chakraborti et al.,<sup>[26]</sup> employing the potassium salt of thiophenol in *N*-methyl-2-pyrrolidone at

Scheme 1. Synthesis of 2-alkynyloxy-BTA derivatives **2** and **9**.

150 °C. The final alkylation step of the phenol derivatives **7** and **8** was found to be a difficult transformation. Modifying the reaction conditions led to moderate yields of the products **2** and **9** (42 and 17%, respectively) when caesium as large carbocation in DMF was used. The electronic stabilization of the phenoxide by conjugation coupled with the formation of intramolecular hydrogen bonds affected negatively the nucleophilicity and thereby the reactivity of **7** and **8**. Crystallographic evidence for these strong intramolecular hydrogen-bonding interactions has been reported by Ueyama and co-workers in their study of the deprotonated form of salicylamide derivatives.<sup>[27]</sup>

2-Bromo-BTA **3** was obtained in two steps starting from 2-bromotrimelic acid (**10**), as described by Wallenfels et al. (Scheme 2).<sup>[28]</sup> The triacid **10** was converted into **3** by using 1-ethyl-3-(3-dimethylaminopropyl)carbodiimide (EDC) and *N*-hydroxysuccinimide in DMF in an acceptable 18% yield.

Scheme 2. Synthesis of 2-bromo-BTA derivative **3**.

## Analyses in the Bulk

### DSC Analysis

BTAs **2** and **3** were analysed by DSC, which revealed polymorphism and a liquid-crystalline mesophase over a broad range of temperatures for both derivatives (Table 1; for DSC traces, see the Supporting Information). The heating cycle of **2** presented an exothermic peak

(−2.54 kJ mol<sup>−1</sup>) at 64.1 °C associated with the transition from the solid to the mesomorphic phase. A second exothermic phase transition (−2.14 kJ mol<sup>−1</sup>) was observed at 109.4 °C. The final isotropization (141.1 °C) was associated with a strong exothermic transition with an enthalpy of −5.09 kJ mol<sup>−1</sup>. Three phase transitions were also measured in the cooling cycle. The isotropic liquid formed the mesomorphic phase at 147.5 °C, showing a strong endothermic transition (4.66 kJ mol<sup>−1</sup>). The small endothermic transition (1.75 kJ mol<sup>−1</sup>) at 120.3 °C indicated a change in the mesomorphic organization and the final solidification of **2** at 57.0 °C was associated with a medium intense endothermicity (2.49 kJ mol<sup>−1</sup>).

The heating cycle of **3** presented a very small exothermic peak (−0.48 kJ mol<sup>−1</sup>) indicating the phase transition between the solid and mesomorphic phase at 70.8 °C. Two other phase modifications were observed in the heating cycle: a strong endothermic peak (18.86 kJ mol<sup>−1</sup>) at 146.7 °C followed by a strong exothermic peak (−20.8 kJ mol<sup>−1</sup>) at 209.1 °C. These two transitions might indicate the formation of a partially organized structure during the heating cycle (cold crystallization) and its relative melting. The final isotropization of **3** was reached at 239.5 °C. In the cooling cycle, the isotropic liquid underwent a phase transition (9.00 kJ mol<sup>−1</sup>) towards the mesomorphic phase at 245.2 °C and the final solidification was observed at 69.5 °C, associated with a very small endothermicity (0.4 kJ mol<sup>−1</sup>).

The temperature range of liquid crystallinity for **3** is much larger than the range observed for **1** (Table 1). The liquid crystallinity of **3** resembles that reported by Nuckolls and co-workers for trialkoxy-substituted crowded derivative **11** (Table 1).<sup>[8a]</sup> The presence of an alkynyloxy group in **2** considerably reduced the temperature range of liquid crystallinity in comparison with BTAs **1** and **3**. The enthalpies determined for the transitions of compound **2** resemble those reported for compounds **1** and **11** forming columnar

Table 1. Transition temperatures<sup>[a]</sup> and, in parentheses, the relative enthalpies of different BTA derivatives.

BTA	2nd heating cycle		Transition temp. [°C] ( $\Delta H$ [kJ mol <sup>-1</sup> ])				$\Delta T$ [°C] <sup>[b]</sup>
			1st cooling cycle				
<b>1</b> <sup>[c]</sup>	99 (-12)		205 (-22)				106
<b>2</b>	64.1 (-2.54)	109.4 (-2.14)	141.1 (-5.09)		147.5 (4.66)	120.3 (1.75)	57.0 (2.49)
<b>3</b>	70.8 (-0.48)	146.7 (18.86)	209.1 (-20.8)		245.2 (9.00)		69.5 (0.4)
<b>11</b> <sup>[d]</sup>	98 (-57.1)		294 (-35.1)		247 (5.6)		83 (39.1)

[a] The transition temperatures have an associated error of  $\pm 0.2$  °C. [b] Temperature range of liquid crystallinity calculated from the 2nd heating cycle. [c] Transition temperatures and enthalpy, as reported by Matsunaga et al.<sup>[3]</sup> [d] Transition temperatures and enthalpies, as reported by Nuckolls and co-workers.<sup>[8a]</sup>

liquid crystals. The presence of bromine increases the solid-like behaviour of **3**, whereas the presence of the pentynyloxy group in **2** decreases its melting point and consequentially its phase-transition energies. The enthalpies for the phase transition of **2** are smaller than those for the reference compounds **1** and **11**. In accordance with this data, the temperature for the first observed transition is lower and, in parallel, the range of liquid crystallinity is smaller.

### Polarized Optical Microscopy

Polarized optical microscopy (POM) was carried out on BTAs **2** and **3**. Both BTAs **2** and **3** formed pseudo-conic textures when cooled from their isotropic liquid phases (Figure 2). These textures are characteristic of columnar liquid crystals. The DSC and POM analyses together indicate that 2-substituted BTAs, such as **2** and **3**, present similar mesomorphic behaviour to the unsubstituted BTA **1** and the fully substituted **11**.

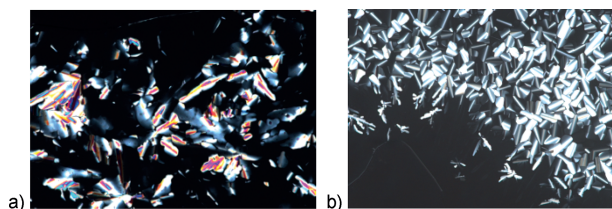


Figure 2. POM micrographs at 100 $\times$  magnification of a) **2** at 137 °C and b) **3** at 202 °C.

### Single-Crystal X-ray diffraction

Chu and co-workers successfully crystallized the *N,N',N''*-trioctyl-BTA derivative reporting a chiral nano-sheet arrangement.<sup>[29]</sup> Unfortunately, compound **2** did not crystallize in our hands. By replacing the hexyl chains by ethyl groups (BTA **9**, Scheme 1), crystals suitable for X-ray diffraction could be obtained by slow evaporation from CDCl<sub>3</sub>. The ethyl-substituted BTA **9** crystallizes in a monoclinic unit cell containing two independent molecules in the asymmetric unit (Figure 3, molecules **α** and **β**, Figure 4, c,d, see the Supporting Information). All three secondary amide groups are involved in two intermolecular hydrogen bonds, as confirmed by the measured C=O $\cdots$ H–N distances

(Table 2, Figure 4, c,d). All three measured amide torsion angles *C*<sub>ortho</sub>–*C*<sub>ipso</sub>–C=O, for both independent molecules **9-α** and **9-β** in the crystal, show significant twisting from coplanarity. The conformation of the amide group in *N*-alkylbenzamides is usually coplanar giving an optimal overlap between the aromatic  $\pi$  system and the  $\pi$  orbitals of the amide group (see the Supporting Information). One of the N–H groups in the *ortho* position of **9** (N1 for **α** and N4 for **β**, Figure 3 and Figure 4, c,d) additionally forms an intramolecular hydrogen bond with the oxygen of the pentynyloxy group (Figure 3, magenta dashed lines; Figure 4, c,d, red dashed lines; Figure 5 magenta dashed lines, see Table 2).

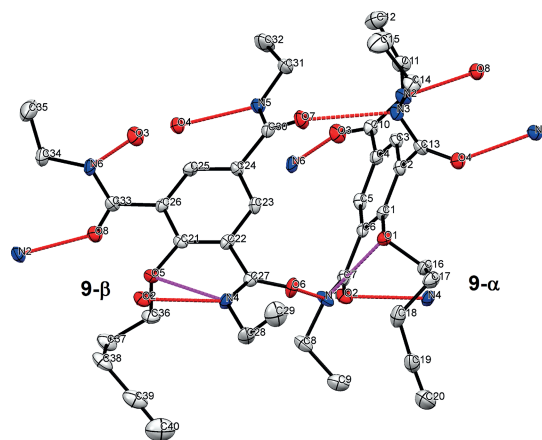


Figure 3. Crystal structures of **9-α** and **9-β**. Hydrogen atoms have been omitted for clarity. Red dashed lines indicate intermolecular hydrogen bonds. Blue dashed lines indicate intramolecular hydrogen bonds. Oxygen atoms are highlighted in red and nitrogen atoms are highlighted in blue.

The amides in the *ortho* position, not involved in intramolecular hydrogen bonds (N3 for **α** and N6 for **β**), show an unusually large torsion angle between the amide group and the plane of the aromatic ring (ca. 60°, twice as big as the other torsion angles, see Table 2). The occurrence of a larger dihedral angle on “crowded arenes” has already been postulated by Nuckolls and co-workers.<sup>[8a]</sup> Our crystallographic results are in agreement with his hypothesis and molecular modelling calculations.

The two *ortho*-amide groups point in the same direction (same sign of the dihedral angle) with respect to the plane of the aromatic ring (same helicity of the propeller-like ar-

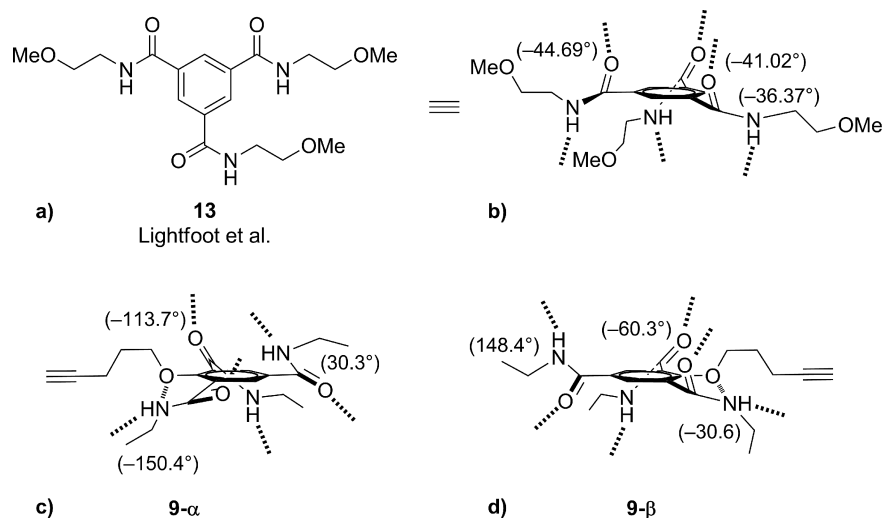


Figure 4. a) Structure of the model compound **13** reported by Lightfoot et al.<sup>[7a]</sup> and b) schematic representation of its X-ray structure. All the carbonyl groups are oriented towards the same face with respect to the aromatic plane. c,d) Schematic representations of the X-ray structures of **9- $\alpha$**  and **9- $\beta$** . The dihedral angles of the amide groups with respect to the main plane of the aromatic core are indicated. Red dashed lines indicate intramolecular hydrogen bonds and black dashed lines indicate intermolecular hydrogen bonds.

Table 2. Hydrogen bond lengths of molecules **9- $\alpha$**  and **9- $\beta$** .

Molecule	Donor (N-H)	Acceptor (C=O)	$d$ [Å] <sup>[a]</sup>	Dihedral angle $\theta$ [°] <sup>[b]</sup>
<b>9-<math>\alpha</math></b>	N1	O6	2.10(3)	C1-C6-C7-O2 -150.4(3)
	N2 <sup>[c]</sup>	O8	1.94(3)	C5-C4-C10-O3 30.3(4)
	N3	O7	2.06(3)	C3-C2-C13-O4 -113.7(3)
<b>9-<math>\beta</math></b>	N4	O2	2.12(3)	C23-C22-C27-O6 -30.6(4)
	N5 <sup>[c]</sup>	O4	2.12(3)	C25-C24-C30-O7 148.4(3)
	N6	O3	2.07(3)	C21-C26-C33-O8 -60.3(4)
Intramolecular hydrogen bond				
<b>9-<math>\alpha</math></b>	NH1	O1	2.30(3)	N1-H1-O1 119(2) <sup>[d]</sup>
<b>9-<math>\beta</math></b>	NH4	O5	2.27(3)	N4-H4-O5 119(2) <sup>[d]</sup>

[a] The distance  $d$  refers to the H $\cdots$ O bond. [b] The sign of the amide dihedral angles indicates the orientation of the carbonyl (C=O) of the amide group with respect to the aromatic plane. For a columnar assembly all of the amide groups have to be directed in the same orientation, leading to the same helicity of the hydrogen-bonding network. [c] This interaction generates a sheet arrangement between the two independent molecules **9- $\alpha$**  and **9- $\beta$** . [d] Measured angle of the intramolecular hydrogen bond.

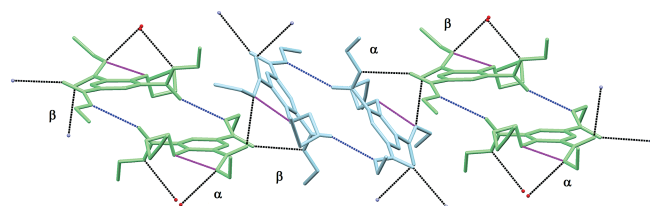


Figure 5. X-ray structure of the pseudo-sheet formed by **9**. Hydrogen atoms have been omitted for clarity. Magenta dashed lines refer to intramolecular hydrogen bonds and blue dashed lines refer to intermolecular hydrogen bonds generating sheet aggregation. The dimer sheet aggregates, indicated by the same colour (light green and light blue) arise exclusively from NH5 $\cdots$ O4 and NH2 $\cdots$ O8 hydrogen bonds. Black dashed lines refer to intermolecular hydrogen bonds generating quasi-orthogonal aggregates.

rament), whereas the *para*-amide group points in the opposite direction. This switch of directionality of the amide groups is in contrast with the BTA model derivative **13** reported in the literature, which forms columnar mesophases (Figure 4, a,b, see the Supporting Information). The asymmetric unit contains two independent molecules,  $\alpha$  and  $\beta$ , arranged in pseudo-sheets in the crystal lattice (Figure 5). Both molecules have the maximum number of six intermolecular hydrogen bonds each (Figure 5, blue and black dashed lines). In addition to these intermolecular hydrogen bonds, one intramolecular hydrogen bond is formed between one of the *ortho*-amide groups (N-H) and the oxygen of the alkyloxy group (see Table 2, Figure 5, magenta dashed lines). Only two out of the six intermolecular hydrogen bonds contribute to the sheet packing (NH5 $\cdots$ O4 and NH2 $\cdots$ O8, see Table 2 and Figure 5, blue dashed lines). These intermolecular interactions generate dimeric aggregates in which the molecules are almost coplanar (the intraplanar dihedral angle is ca. 4°, see Figure 5 and the Supporting Information). This arrangement allows  $\pi$ - $\pi$  interactions thereby potentially enabling columnar organizations. The other four intermolecular interactions (Figure 5, black dashed lines) are directed out of the sheet plane generating an orthogonal packing that deviates from the potential columnar arrangement (no  $\pi$ - $\pi$  stacking). The formation of the intramolecular hydrogen bond perturbs the regular growing of the sheet aggregates.

Despite the significant differences between the crystal structure of **9** and the structure of the model BTA **13**, a liquid crystalline phase has been observed for **2**. Therefore an analysis of the thermodynamic parameters of the self-assembly process in solution was needed to elucidate quantitatively the effect of the additional substituent on the formation of intermolecular hydrogen bonds in an effort to rationalize the differences found between **1**, **2** and **3** in the liquid-crystalline state.

## Analyses in Dilute Solution

Variable-Concentration  $^1\text{H}$  NMR Dilution Experiments

$^1\text{H}$  NMR experiments were performed at different concentrations of **2** and **3** in  $[\text{D}_2]$ dichloromethane as the solvent to measure the association constant  $K_a$ . BTA **1** was chosen as the reference compound. The association process has been well studied and is described in the literature.<sup>[13b]</sup> We chose  $[\text{D}_2]$ dichloromethane to minimize the hydrogen-bond-donor or -acceptor effects that occur with other solvents such as  $\text{CDCl}_3$  or  $[\text{D}_6]\text{DMSO}$ . The  $^1\text{H}$  NMR spectra of BTA **1** were recorded at 295 K in a concentration range varying from 0.39 to 202 mM (Figure 6).

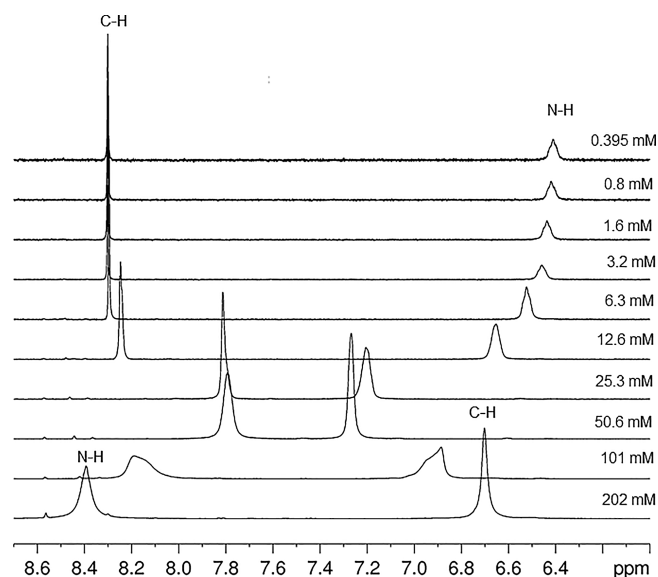


Figure 6. Variable-concentration  $^1\text{H}$  NMR spectra of **1** in  $\text{CD}_2\text{Cl}_2$  at 295 K. The NMR spectra were recorded by decreasing the concentration from 202.3 to 0.395 mM. Only the aromatic region between 8.7 and 6.5 ppm is presented.

Upon increasing the concentration, a large downfield shift of the N–H signals ( $\Delta\delta \approx 2$  ppm) was observed. On the other hand, a large upfield shift of the aromatic protons

was measured ( $\Delta\delta \approx 1.6$  ppm) over the same concentration range. A concentration-induced variation of the  $^1\text{H}$  NMR chemical shift of BTA **2** was also observed at 295 K in  $\text{CD}_2\text{Cl}_2$  (Figure 7). The presence of the pentynyloxy substituent on the aromatic ring causes a reduction of the symmetry of the molecule ( $C_{2v}$ ), generating two distinct signals for the N–H group of the three amides. For the sake of clarity, these signals are referred to as N–H<sub>ortho</sub> and N–H<sub>para</sub> respectively (see Scheme 3). Increasing the concentration (from 0.77 to 198 mM) caused an upfield shift of the aromatic protons ( $\Delta\delta = 0.21$  ppm) and a downfield shift of both types of N–H protons (N–H<sub>ortho</sub>  $\Delta\delta = 0.281$  ppm, N–H<sub>para</sub>  $\Delta\delta = 0.59$  ppm). The  $\Delta\delta$  values are considerably smaller than those observed for BTA **1**. The  $\Delta\delta$  values for the N–H<sub>ortho</sub> and the C–H protons of the aromatic ring are similar, whereas the  $\Delta\delta$  value for the N–H<sub>para</sub> proton is twice as large, but still almost a factor of four less than that of BTA **1**. The bromo-BTA derivative **3** has a very low solubility in  $\text{CD}_2\text{Cl}_2$  and we were forced to replace  $[\text{D}_2]$ -

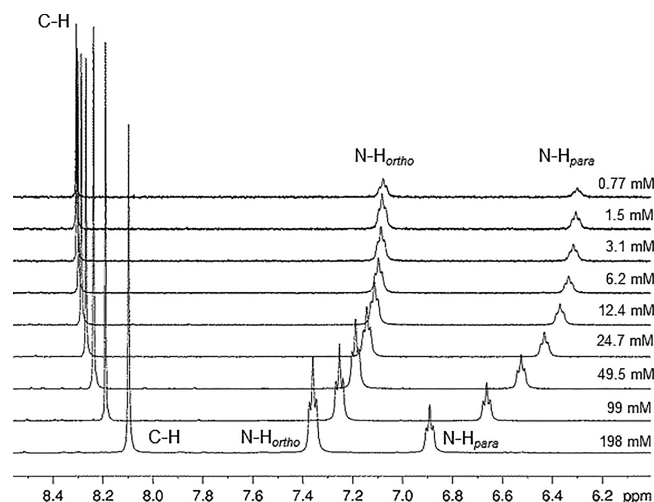
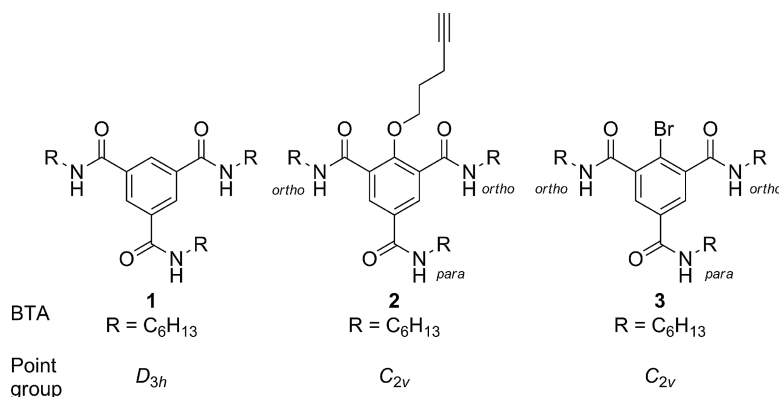


Figure 7. Variable-concentration  $^1\text{H}$  NMR spectra of **2** in  $\text{CD}_2\text{Cl}_2$  at 295 K. The NMR spectra were recorded by decreasing the concentration from 198 to 0.77 mM. In the figure only the aromatic region (8.5–6.0 ppm) is presented.



Scheme 3. Comparison of the different BTA structures **1–3**. The reduced symmetry in 2-substituted BTA **2** and **3** generates two distinct signals of the amide protons (N–H<sub>ortho</sub> and N–H<sub>para</sub>).

dichloromethane with  $[D_1]$ chloroform. As in the case of BTA **2**, the N–H signals are referred to as N–H<sub>ortho</sub> and N–H<sub>para</sub> (see Scheme 3). By increasing the concentration from 0.10 to 82 mM, a large upfield shift for the C–H protons ( $\Delta\delta = 0.95$  ppm) was observed and a very large downfield shift was observed for the N–H protons of the amides (N–H<sub>ortho</sub>  $\Delta\delta = 2.45$  ppm, N–H<sub>para</sub>  $\Delta\delta = 2.53$  ppm, Figure 8). The  $\Delta\delta$  values for both types of N–H protons are even larger than those observed for compound **1**, whereas the  $\Delta\delta$  value for the aromatic C–H was almost a factor of two smaller than the values observed for our reference compound. The NMR spectra of **3** show extensive line-broadening at certain concentrations, probably due to the intermediate exchange rate of the association of **3**.

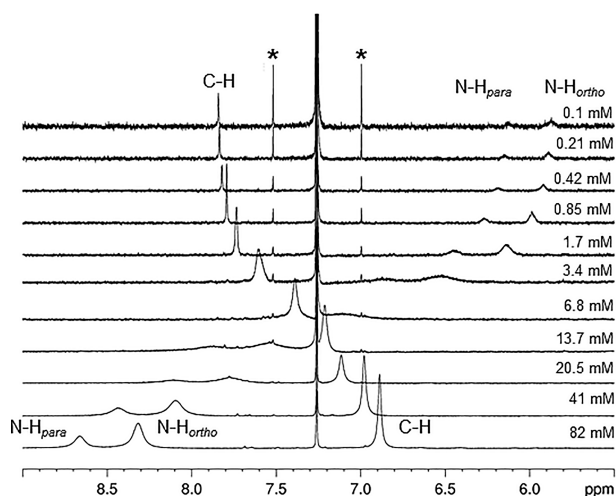


Figure 8. Variable-concentration  $^1\text{H}$  NMR spectra of **3** in  $\text{CDCl}_3$  at 295 K. The NMR spectra were recorded by decreasing the concentration from 82 to 0.10 mM. In the figure only the aromatic region (9.0–5.0 ppm) is presented. \* The asterisks indicate the  $^{13}\text{C}$  satellite signals of the residual  $\text{CHCl}_3$  in the NMR solvent.

Globally, the observed concentration-induced upfield shifting of the aromatic protons is coherent with the enhancement of  $\pi$ – $\pi$  interactions. According to the X-ray structures of the model tris(2-methoxyethyl)-BTA derivative **13** (see the Supporting Information), the short inter-ring distance (3.62 Å) enables strong aromatic interactions ( $\pi$ – $\pi$  stacking) along the columnar axis of the mesophase resulting in an upfield ring-current shift of the aromatic protons. In the case of the amide protons, the observed concentration-induced downfield shifting is consistent with the formation of intermolecular hydrogen-bonding interactions. The presence of a bulky atom, such as bromine, influences the amide torsion angle. The carbonyls of the amides are forced out of planarity despite the concomitant loss of conjugation. In the case of BTA **2**, the concentration-induced shift of the N–H<sub>ortho</sub> protons is two-fold smaller than the shifts of the N–H<sub>para</sub> proton and four-fold smaller than the shifts observed for the reference compound **1**. In an effort to explain this observation, we invoked the formation of intramolecular hydrogen bonds by the N–H<sub>ortho</sub> protons of **2**. The dilution experiments are compatible with the pres-

ence of such an intramolecular hydrogen bond not only in the pure material but also in solution.

### $^1\text{H}$ DOSY NMR Study

To complete the analysis of the aggregation of our BTA derivatives in solution,  $^1\text{H}$  2D-DOSY experiments were executed. As for the variable-concentration  $^1\text{H}$  NMR experiments, BTA **1** was selected as the reference compound for the 2D DOSY experiments and  $[D_2]$ dichloromethane was used as the solvent. For all three BTAs **1–3**, a reduction of the diffusion coefficient was observed upon increasing the concentration (Figures 9–11 and Table 3).

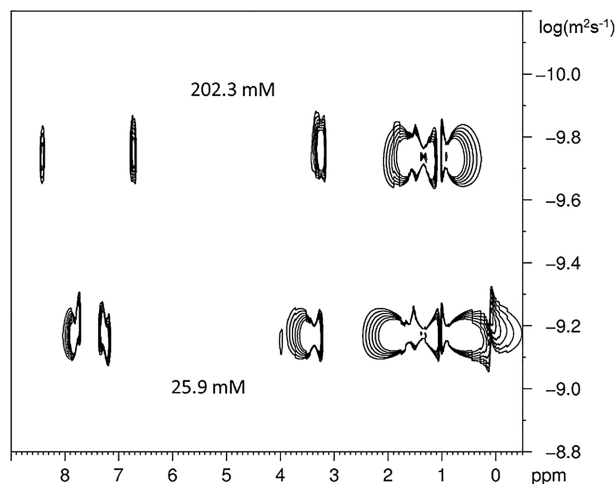


Figure 9.  $^1\text{H}$  2D DOSY spectra of **1** in  $\text{CD}_2\text{Cl}_2$  at a concentration of 202.3 and 25.9 mM. The spectra were recorded at 295 K.

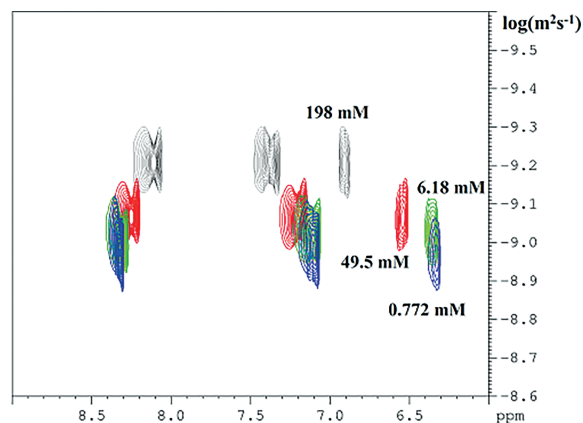


Figure 10.  $^1\text{H}$  2D DOSY spectra of **2** in  $\text{CD}_2\text{Cl}_2$  at 198 (in grey), 49.5 (in red), 6.18 (in green), and 0.772 mM (in blue) recorded at 295 K.

These results are consistent with the formation of supramolecular aggregates, which diffuse more slowly than the monomeric species. In the DOSY spectrum of 13.7 mM of **3**, the signals of the amide protons are broad, whereas the aromatic proton signal partially overlaps with the residual signal of  $\text{CHCl}_3$ . These experimental difficulties hamper the precise measurement of the diffusion coefficient from these signals. However, the diffusion coefficient of the molecule can be measured from the analysis of the signals in the ali-

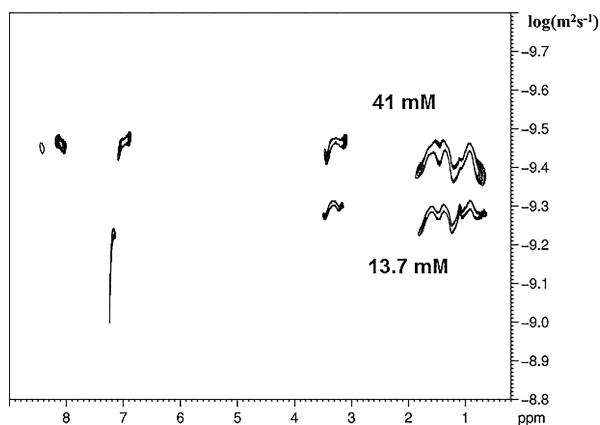


Figure 11.  $^1\text{H}$  2D DOSY spectra of **3** in  $\text{CD}_2\text{Cl}_2$  at 41 and 13.7 mM. The spectra were recorded at 295 K.

Table 3. Observed diffusion coefficients  $D$  for BTA 1–3 at different concentrations.

	BTA 1		BTA 2			BTA 3		
[BTA] <sup>[a]</sup>	202.3	25.9	198	49.5	6.18	0.772	41	13.7
$D_{\text{obs}}$ <sup>[b]</sup>	-9.79	-9.19	-9.23	-9.08	-9.02	-8.89	-9.46	-9.22
$\chi_{\text{mon}}$ <sup>[c]</sup>	0.03	0.58 <sup>[d]</sup>	0.40	0.77	0.96	0.994	0.14	0.35

[a] BTA concentrations in mmol/L. [b] Diffusion coefficients measured as  $\log(\text{m}^2\text{s}^{-1})$ . [c] The molar fractions of the monomer species  $\chi_{\text{mon}}$  were obtained based on the extrapolated limiting value (see the Supporting Information) obtained from the fitting curves (see Figures 12, 13 and 14). [d] Extrapolated values (see the Supporting Information).

phatic region of the spectrum (Figure 11). The observed chemical shift  $\delta_{\text{obs}}$  is the weighted average of the chemical shifts of the monomeric species ( $\delta_{\text{mon}}$ ) and the aggregated species ( $\delta_{\text{agg}}$ ) according to Equation (1)

$$\delta_{\text{obs}} = \delta_{\text{mon}}\chi_{\text{mon}} + \delta_{\text{agg}}\chi_{\text{agg}} \quad (1)$$

in which  $\chi_{\text{mon}}$  and  $\chi_{\text{agg}}$  are the fractions of monomer and aggregate, respectively, and  $\chi_{\text{mon}} + \chi_{\text{agg}} = 1$ . Similarly, the observed diffusion coefficient  $D_{\text{obs}}$  is the weighted average of the diffusion coefficient of the monomer ( $D_{\text{mon}}$ ) and the aggregate ( $D_{\text{agg}}$ ), respectively, according to Equation (2).

$$D_{\text{obs}} = D_{\text{mon}}\chi_{\text{mon}} + D_{\text{agg}}\chi_{\text{agg}} \quad (2)$$

The limiting values of  $\delta_{\text{mon}}$  and  $\delta_{\text{agg}}$  can be extrapolated from the curve fitting (Figure 12, 13 and 14).

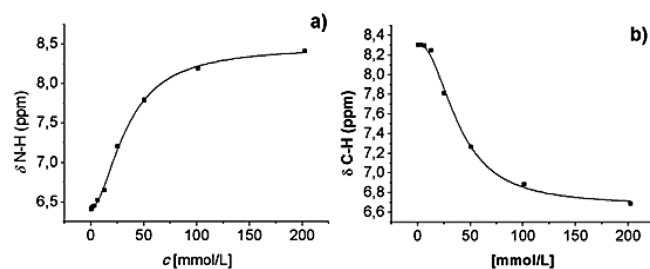


Figure 12. Curves fitted according to Equation (3) for the plot  $\delta$  vs. [1]. a) N–H protons and b) C–H aromatic protons.

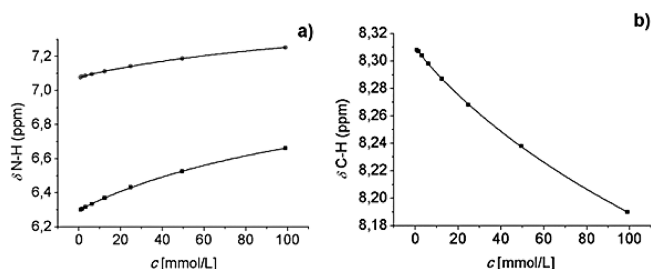


Figure 13. Curves fitted according to Equation (3) for the plot  $\delta$  vs. [2]. a) N–H protons: ● indicate N–H<sub>ortho</sub> signals and ■ indicate N–H<sub>para</sub> signals. b) C–H aromatic protons. In both curves the asymptotes, indicating full aggregation, are not reached due to a weakness of the binding.

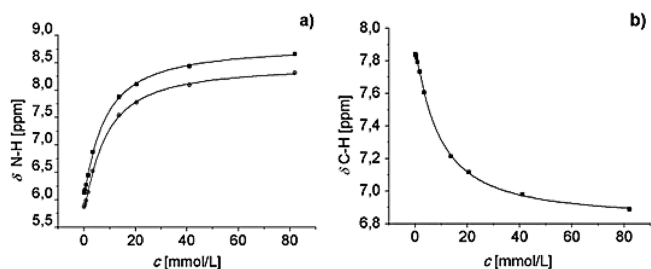


Figure 14. Curves fitted according to Equation (3) for the plot  $\delta$  vs. [3]. a) N–H protons: ● indicate N–H<sub>ortho</sub> signals and ■ indicate N–H<sub>para</sub> signals. b) C–H aromatic protons.

Assuming complete aggregation ( $\chi_{\text{agg}} = 1$ ) and complete disaggregation ( $\chi_{\text{mon}} = 1$ ) at the two limits of the fitting curves, an estimation of the ratio (molar fraction  $\chi$ ) of the aggregate and the monomer can be obtained for the measured experimental points. The monomer molar fraction  $\chi_{\text{mon}}$  was calculated based on the measured shift of the N–H signal. In the case of BTAs 2 and 3, the calculation was carried out based on the shift of the N–H<sub>para</sub> signal being exclusively due to intermolecular hydrogen-bonding interactions (Table 3).

### Simulation of the Aggregation Process

The concentration-induced chemical shifts were fitted according to a non-linear least-squares equation. Meijer and co-workers elaborated a fitting equation to interpolate isodesmic aggregation curves, specifically excluding cooperativity.<sup>[30]</sup> However, BTA 1 is known to aggregate according to a cooperative mechanism characterized by a nucleation step ( $K_n$ ) and an elongation step ( $K_e$ ). Therefore the general fitting procedure based on a logistic fitting function using the OriginPro8<sup>®</sup> program<sup>[32]</sup> [ $\delta_{\text{C-H}}$  and  $\delta_{\text{N-H}}$  vs. [BTA], Equation (3)] was used, giving a considerably better fit (correlation coefficients above 0.99).

$$\delta_{\text{obs}} = \delta_{\text{agg}} + \frac{(\delta_{\text{mon}} - \delta_{\text{agg}})}{\left[1 + \left(\frac{c}{K_d}\right)^p\right]} \quad (3)$$

In Equation (3),  $c$  is the total concentration of the BTA,  $p$  is the slope factor of the fitting curve,  $\delta_{\text{mon}}$  and  $\delta_{\text{agg}}$  are,

Table 4. Thermodynamic data for the aggregation of BTAs 1–3 calculated at 295 K by applying the logistic fitting equation and the isodesmic fitting model.

Logistic <sup>[a]</sup>	BTA 1		BTA 2			BTA 3		
	N–H	C–H	N–H <sub>ortho</sub>	N–H <sub>para</sub>	C–H <sub>arom.</sub>	N–H <sub>ortho</sub>	N–H <sub>para</sub>	C–H <sub>arom.</sub>
$K_d$ [mM]	34 (1)	39 (2)	196(53)	176(30)	337 (117)	8.4(3)	8.0(4)	9.3(2)
$K_a$ [M <sup>-1</sup> ]	29(4)	26(5)	5(1)	6(1)	3(1)	119(4)	125(6)	108(2)
$R_2$	0.9985	0.9968	0.9998	0.9999	0.9999	0.9994	0.9993	0.9998
$p$	1.8(1)	2.2(2)	0.91(4)	0.94(3)	0.90(4)	1.22(5)	1.16(5)	1.19(3)
$\Delta G^{[d]}$ [kJ mol <sup>-1</sup> ]	-8.3 (1)	-8.0 (1)	-4.0(7)	-4.3(4)	-2.7(9)	-11.7(1)	-11.8(1)	-11.5(1)
Isodesmic <sup>[b]</sup>								
$K_a$ [M <sup>-1</sup> ]	15(6) <sup>[c]</sup>	10(5) <sup>[c]</sup>	4.7(3)	4.5(2)	3.3(2)	109(25)	120(25)	98(20)
$R_2$	0.9728	0.9584	0.9998	0.9999	0.9998	0.9909	0.9927	0.9928
$\Delta G^{[d]}$ [kJ mol <sup>-1</sup> ]	-7(1)	-6(1)	-3.8(2)	-4(1)	-2.9(1)	-11.5(6)	-11.7(5)	-11.3(5)

[a] Calculated from the fitting procedure using Equation (3). [b] Calculated from the fitting procedure using Equation (4). [c] The values calculated for **1** by applying the isodesmic model have a low correlation coefficient ( $R_2$ ), which indicates low quality of fit. [d] Gibbs free energy.

respectively, the extrapolated values of the chemical shifts for the monomer at infinite dilution and the chemical shift for the aggregate obtained by the fitting procedure, and  $K_d$  (mmol L<sup>-1</sup>) is the dissociation constant of the aggregates. The association constants, measured as M<sup>-1</sup>, were calculated based on the relation  $K_a = 1000/K_d$ . If  $p > 1$ , a sigmoidal behaviour of the fitting curve is indicated that is compatible with positive cooperativity, and if  $p < 1$  negative cooperativity is indicated. When  $p = 1$ , the curve assumes a hyperbolic behaviour, which indicates the absence of cooperativity. This statistical data fitting was applied to the concentration-dependent NMR data of **1**. The best fit (Figure 12, a,b) gave a sigmoidal curve with positive cooperativity, as indicated by the slope factor of 1.8(1) for N–H and of 2.2(2) for C–H (Table 4). The result of the statistical data analysis shows cooperativity for the aggregation of **1**, in agreement with the findings reported in the literature.<sup>[13b]</sup> As our NMR results for **1** are compatible with the conclusion reported in the literature, we deduced that our procedure is suitable for the analysis of the aggregation behaviour of BTA derivatives. The values of  $K_a$ , 29 M<sup>-1</sup> determined by using the shifts of the N–H signals and 26 M<sup>-1</sup> deduced by using the shifts of the C–H aromatic signals, are, to all intent and purposes, sufficiently similar such that we can assume that the aggregation observed by monitoring the two separate sensors is the same association process. The observed association constants  $K_a$  for the three studied compounds decrease in the order **3** > **1** > **2** (Table 4). The relative strength of the association constant  $K_a$  follows the same trend as the material property expressed as the temperature range of the liquid-crystalline phase observed by DSC (Table 1).

The unsubstituted BTA **1** has been carefully studied and characterized. Therefore we used BTA **1** as the reference compound in our studies. The association constant  $K_a$  of 2-pentynyloxy-BTA **2** is significantly smaller than that of **1** (about six- to eight-fold smaller). On the other hand, the value of  $K_a$  determined for the association of **3** is four-fold larger than that of **1** (Table 4). The calculated difference in  $\Delta G$  ( $\Delta G = -RT \ln K_a$ ) between **1** and **2** (4.3 kJ mol<sup>-1</sup> from the N–H<sub>ortho</sub>, 4.0 kJ mol<sup>-1</sup> from N–H<sub>para</sub> and 5.3 kJ mol<sup>-1</sup>

from C–H) is compatible with the loss of one hydrogen-bonding interaction in **2**.

This observation supports the hypothesis that the formation of an intramolecular hydrogen bond in **2** destabilizes the columnar assembly, tentatively attributed to the occurrence of a competing intramolecular hydrogen bond. The presence of bromine in **3** significantly stabilizes the columnar association process. The large dihedral angle of at least one of the amide groups relative to the plane of the aromatic ring in BTA **3** may enhance the formation of intermolecular hydrogen bonds. The increase in this dihedral angle has been invoked as an argument for the reinforced strength of the self-assembly.<sup>[8a]</sup> The slope factors obtained from the fitting of the curves of the experimental data for **2** and **3** gave  $p$  values close to 1 (Table 4), which indicates no or only small cooperativity. For compounds **2** and **3**, the use of the isodesmic model [Equation (4)] for the fitting process gave results that cannot be distinguished from the results obtained by the more general approach using logistic fitting.<sup>[30]</sup>

$$\delta_{obs} = \delta_{mon} + (\delta_{agg} - \delta_{mon}) \left[ 1 + \frac{(1 - \sqrt{4K_a c + 1})}{2K_a c} \right] \quad (4)$$

As indicated, the application of Equation (4) to the NMR data of **1** resulted in poorer data fitting due to the cooperativity effects described (see Table 4 and the Supporting Information).

## Conclusions

The mono-core-functionalized BTA derivatives **2** and **3** form columnar mesophases over a broad temperature range. By using the  $C_{3v}$ -symmetric molecule **1** as a reference compound, the thermodynamics of the supramolecular assembly process could be analysed by a variable-concentration <sup>1</sup>H NMR analysis. Concentration-dependent chemical shifts together with the results of DOSY experiments allowed the determination of the thermodynamics of the supramolecular aggregation process and differentiation be-

tween isodesmic and cooperative self-assembly. The introduction of the pentynyloxy group, a hydrogen-bond-acceptor substituent, into the BTA derivative **2** reduced the temperature range of the liquid crystalline phase and the strength of the aggregation process in solution. Both of these observations are compatible with the destabilization of the supramolecular assembly, formed through intermolecular hydrogen bonds, by the formation of an intramolecular hydrogen-bonding interaction. The introduction of bromine onto the BTA aromatic core efficiently stabilized the columnar organization and increased the strength of the aggregation in solution. In both cases, the functionalization of the aromatic core induced the loss of cooperativity during the supramolecular assembly process. The BTA derivatives **2** and **3** were found to aggregate according to an isodesmic self-assembly process.

## Experimental Section

**General:** Reactions requiring anhydrous conditions were performed in oven-dried (120 °C) glassware under dry N<sub>2</sub> or dry Ar. Anhydrous solvents such as toluene ( $\geq 99.7\%$ ,  $\leq 0.005\%$  H<sub>2</sub>O), DMF ( $\geq 99.8\%$ ,  $\leq 0.01\%$  H<sub>2</sub>O), DMSO ( $\geq 99.5\%$ ,  $\leq 0.005\%$  H<sub>2</sub>O), THF ( $\geq 99.5\%$ ,  $\leq 0.025\%$  H<sub>2</sub>O, stabilized with 0.025% 2,6-di-*t*Bu-4-methylphenol) were obtained from Aldrich and stored over molecular sieves. *N*-Methylpyrrolidone (NMP) was purchased from Acros (purity 99%). Brine refers to a satd. aq. solution of NaCl. Petroleum ether refers to the boiling fraction of 40–60 °C. All other solvents were of technical grade and used without further purifications. <sup>1</sup>H and <sup>13</sup>C NMR spectra were recorded with Bruker Avance II-400 (400.13 MHz, <sup>1</sup>H; 100.61 MHz, <sup>13</sup>C) and DPX 400 (400.13 MHz, <sup>1</sup>H; 100.61 MHz, <sup>13</sup>C) spectrometers at the Neuchâtel Platform of Analytical Chemistry (NPAC) of the University of Neuchâtel. Chemical shifts ( $\delta$ ) are quoted in ppm and are given relative to tetramethylsilane ( $\delta = 0$  ppm) as the internal standard or the residual solvent peak of CDCl<sub>3</sub> ( $\delta = 7.26$  ppm, <sup>1</sup>H;  $\delta = 77.0$  ppm, <sup>13</sup>C), dichloromethane ( $\delta = 5.32$  ppm, <sup>1</sup>H;  $\delta = 53.84$  ppm, <sup>13</sup>C), methanol ( $\delta = 3.31$  ppm, <sup>1</sup>H;  $\delta = 49.00$  ppm, <sup>13</sup>C), DMSO ( $\delta = 2.50$  ppm, <sup>1</sup>H;  $\delta = 39.52$  ppm, <sup>13</sup>C). All the deuteriated NMR solvents were purchased from Cambridge Isotope. Multiplicities are indicated by s (singlet), d (doublet), t (triplet), q (quartet), m (multiplet) and br. (broad). Coupling constants, *J*, are reported in Hz. The assignments were verified by the following 2D experiments if necessary: HSQC, HMBC and COSY. <sup>1</sup>H 2D-COSY experiments were performed by stimulated echo and LED schemes using bipolar gradient pulses for diffusion and two spoil gradients. The strength of the diffusion gradients was varied from 5 to 95% in 32 increments. Typically, 8 to 32 scans were recorded for each increment.<sup>[31]</sup> The lengths of the diffusion and spoil gradients were 2 and 1.1 ms, respectively, with a gradient recovery time of 200  $\mu$ s. The data matrix was 4K  $\times$  32 in the time domain and 4K  $\times$  512 in the processed domain. Mass spectrometry was performed at the NPAC of the University of Neuchâtel. Electrospray [ESI (+/–)] MS was performed with an API 4000 QTrap ABSciex or LC/MSD Trap Agilent spectrometer. The LC–MS retention times (*R*<sub>t</sub>) and low-resolution MS were recorded with a UPLC Ultimate 3000 Dionex – API 4000 QTrap, ABSciex instrument. The solvents were of UPLC grade and water was Milli-Q® grade. High-resolution mass spectra were recorded with a Bruker FTMS 4.7T BioAPEX II FT/ICR spectrometer by using a standard electrospray ion (ESI) or MALDI source at the University of Fribourg (Switzerland). IR spectra were

recorded with a Perkin–Elmer Spectrum One FT-IR version B spectrophotometer using the Perkin–Elmer Spectrum™ 5 software<sup>[33]</sup> for recording and treating the data. Peaks are reported in cm<sup>–1</sup> with relative intensities indicated as follows: s (strong, 67–100%), m (medium, 34–66%) and w (weak, 0–33%). Solid samples were measured in freshly prepared KBr pellets. Liquids were measured as films using polished KBr plates. Melting points were determined by using a Gallenkamp MPD 350-BM capillary melting-point apparatus in open tubes. Analytical TLC was performed on Merck silica gel plates [aluminium sheets pre-coated with silica (60 F254)] or on Merck aluminium oxide plates [aluminium sheets pre-coated with aluminium oxide (60 F254)]. Visualization was accomplished with UV light unless noted otherwise. Flash column chromatography was performed by using silica gel (Brunschwing Silica gel 60, 32–63 or Brunschwing Silica gel 60, 63–200). All reaction temperatures refer to oil bath temperatures measured with Heidolph EKT 3 mA® thermocouples unless specifically mentioned otherwise. DSC analyses were accomplished with a Mettler Toledo DSC1 STARe® instrument. The samples were prepared in an aluminium sampler. Each analysis refers to three heating–cooling cycles performed at 10 °C min<sup>–1</sup> under nitrogen flux. The reported temperatures refer to the “onset” peak. Data were analysed by using STARe software. POM analyses were performed with an Axio Scope Zeiss microscope. Samples were heated on a Linkam THMS600® heater controlled by a Linkam 93 apparatus. POM images were taken by using a Fujix Digital Camera HC-300Z® and processed with the AxioVision Rev 4.8® program.

**N<sup>1</sup>,N<sup>3</sup>,N<sup>5</sup>-Trihexylbenzene-1,3,5-tricarboxamide (1):** Benzene-1,3,5-tricarboxyl trichloride (1 g, 3.77 mmol) was dissolved in dry THF (6 mL) and the solution was added dropwise to a solution of hexylamine (2.3 mL, 30.1 mmol) in dry THF (6 mL) at 0 °C under nitrogen. The reaction mixture was stirred at 0 °C for 30 min and at room temperature for another 18 h. The organic solvent was removed under vacuum and the crude solid was diluted with 2 M HCl (15 mL). The product was extracted with ethyl acetate. The resulting organic solution was washed again with 2 M HCl, 5% sol. of NaHCO<sub>3</sub> and brine. The organic phase was dried with MgSO<sub>4</sub> and the solvent was removed under vacuum. The product was purified by chromatography on silica gel using cyclohexane/ethyl acetate (1:1) as eluent to afford 1.125 g of **1** as an amorphous white solid in 65% yield. *R*<sub>f</sub> (SiO<sub>2</sub>, cyclohexane/ethyl acetate, 1:1) = 0.55. <sup>1</sup>H NMR (CDCl<sub>3</sub>, 400 MHz, 295 K):  $\delta = 8.32$  (s, 3 H, Ar-*H*), 6.56 (t, <sup>3</sup>*J*<sub>H,H</sub> = 4.5 Hz, 3 H, NH), 3.45 (q, <sup>3</sup>*J*<sub>H,H</sub> = 6.7 Hz, 6 H, CH<sub>2</sub>NH), 1.60 (quint., <sup>3</sup>*J*<sub>H,H</sub> = 7.2 Hz, 6 H, CH<sub>2</sub>CH<sub>2</sub>NH), 1.39–1.31 (m, 18 H, CH<sub>2</sub>), 0.89 (t, <sup>3</sup>*J*<sub>H,H</sub> = 6.5 Hz, 9 H, CH<sub>3</sub>) ppm. <sup>13</sup>C NMR (CDCl<sub>3</sub>, 100 MHz, 295 K):  $\delta = 165.8, 135.4, 128.1, 40.5, 31.6, 29.6, 26.8, 22.7, 14.2$  ppm.

**2-Methoxybenzene-1,3,5-tricarboxylic Acid (4):** Compound **4** was prepared according to the procedure previously reported by Raymond and co-workers.<sup>[27]</sup> 2,6-Bis(hydroxymethyl)-4-methylphenol (10 g, 59.4 mmol) was dissolved in acetone (200 mL). Anhydrous K<sub>2</sub>CO<sub>3</sub> (12.32 g, 89.175 mmol) was added and the suspension was stirred for 5 min. Me<sub>2</sub>SO<sub>4</sub> (6.8 mL, 71.3 mmol) was added and the reaction was stirred at 70 °C for 15 h. The solid was filtered off and the solvent evaporated under vacuum to afford a crude white solid product. The product was purified by recrystallization from ethyl acetate to afford 6.4 g of a white solid in 60% yield. *R*<sub>f</sub> (SiO<sub>2</sub>, ethyl acetate/petroleum ether, 9:1) = 0.57, m.p. 107 °C. <sup>1</sup>H NMR (CDCl<sub>3</sub>, 400 MHz, 295 K):  $\delta = 7.14$  (s, 2 H, Ar-*H*), 4.71 (s, 4 H, CH<sub>2</sub>), 3.84 (s, 3 H, OMe), 2.32 (s, 3 H, Me), 1.94 (s, 2 H, OH) ppm. <sup>13</sup>C NMR (CDCl<sub>3</sub>, 100 MHz, 295 K):  $\delta = 165.8, 153.8, 134.3, 133.5, 124.3, 115.9, 62.2, 60.9, 20.8$  ppm. MS (ESI): *m/z* (%) = 205.0 (100) [M + Na]<sup>+</sup>.

KOH caps (3.8 g, 67.9 mmol) were added to a solution of (2-methoxy-5-methyl-1,3-phenylene)dimethanol (6.18 g, 33.9 mmol) in distilled water (400 mL) and the mixture was stirred for 10 min.  $\text{KMnO}_4$  (26.83 g, 169.7 mmol) was added portionwise and further distilled water (200 mL) was added. The dark solution was stirred at 100 °C for 7 h. The reaction mixture was cooled to room temperature and  $\text{Na}_2\text{S}_2\text{O}_3$  powder was added until the permanganate was reduced forming a dark-brown suspension. The solid residue was filtered off and the volume of water was reduced to 150 mL by distillation under vacuum. Concentrated HCl (37%) was added until pH 3. The aqueous phase was saturated by adding solid NaCl. The aqueous solution was extracted with AcOEt (4 × 200 mL). The organic phases were dried with  $\text{MgSO}_4$  and the solvent was removed under vacuum. The resulting white solid was dissolved in methanol and the yellowish insoluble solid was filtered off. The solvent was evaporated under vacuum to afford 6.2 g of **4** as a white solid in 76% yield. The crude product was used without further purification.  $^1\text{H}$  NMR (DMSO, 400 MHz, 295 K):  $\delta$  = 8.31 (s, 2 H, Ar-H), 3.85 (s, 3 H, OMe) ppm.  $^{13}\text{C}$  NMR (DMSO, 100 MHz, 295 K):  $\delta$  = 166.6, 166.0, 161.7, 134.8, 128.1, 126.1, 63.5 ppm. MS (ESI):  $m/z$  (%) = 239.1 (100) [M - H] $^-$ .

**$N^1,N^3,N^5$ -Triethyl-2-methoxybenzene-1,3,5-tricarboxamide (5):** 2-Methoxybenzene-1,3,5-tricarboxylic acid (**4**) (500 mg, 2.1 mmol) was suspended in dry toluene (5 mL) and  $\text{SOCl}_2$  (0.53 mL, 7.3 mmol) and 2 drops of DMF were added. The suspension was heated at 110 °C for 2 h. The resulting yellowish solution was cooled to room temperature and the volatile compounds were removed under high vacuum to furnish a pale-yellow oil. The resulting acid chloride was dissolved in THF (5 mL) and added dropwise to a solution of  $\text{EtNH}_2$  (1.15 mL, 14.46 mmol, 70% sol. in water) dissolved in THF (5 mL) at 0 °C. After the complete addition, the reaction mixture was stirred at 0 °C for 1 h and at room temperature for another 4 h. The solution was acidified to pH 3 by adding 2 M HCl. The organic solvent was removed under vacuum and the resulting aqueous solution was diluted with water. The product was extracted with ethyl acetate. The organic phase was dried with  $\text{MgSO}_4$  and the solvent removed under vacuum. The product was purified by chromatography on  $\text{SiO}_2$  using ethyl acetate/methanol (8:2) as eluent to afford 429 mg of **5** as a white solid in 64% yield.  $R_f$  (ethyl acetate/MeOH, 9:1) = 0.5, m.p. 167–168 °C. IR (KBr):  $\tilde{\nu}$  = 3272 (m), 3077 (w), 2977 (m), 2937 (m), 1714 (m), 1644 (s), 1543 (s), 1465 (m), 1300 (s), 1149 (m), 1093 (m), 1057 (w), 1003 (m), 924 (w), 656 (w), 601 (w)  $\text{cm}^{-1}$ .  $^1\text{H}$  NMR ( $\text{CD}_3\text{OD}$ , 400 MHz, 295 K):  $\delta$  = 8.15 (s, 2 H, Ar-H), 3.90 (s, 3 H,  $\text{OCH}_3$ ), 3.47–3.37 (m, 6 H,  $\text{CH}_2\text{-NH}$ ), 1.25 (t,  $^3J_{\text{H,H}} = 7.3$  Hz, 6 H,  $\text{CH}_3$ ) ppm.  $^{13}\text{C}$  NMR ( $\text{CD}_3\text{OD}$ , 100 MHz, 295 K):  $\delta$  = 168.0 (C=O $_{ortho}$ ), 167.7 (C=O $_{para}$ ), 159.0 (C-OMe), 131.9 (Ar), 131.2 (C-C=O $_{para}$ ), 131.0 (C-C=O $_{ortho}$ ), 63.3 ( $\text{OCH}_3$ ), 35.9 ( $\text{CH}_2\text{-NH}$ ), 35.8 ( $\text{CH}_2\text{-NH}$ ), 14.8 ( $\text{CH}_3\text{-CH}_2$ ), 14.7 ( $\text{CH}_3\text{-CH}_2$ ) ppm. MS (ESI):  $m/z$  (%) = 344.3 (100) [M + Na] $^+$ . HRMS (ESI): calcd. for  $\text{C}_{16}\text{H}_{23}\text{N}_3\text{O}_4\text{Na}^+$  344.1581; found 344.1575 [M + Na] $^+$ .

**$N^1,N^3,N^5$ -Triethyl-2-hydroxybenzene-1,3,5-tricarboxamide (7):**  $N^1,N^3,N^5$ -Triethyl-2-methoxybenzene-1,3,5-tricarboxamide (**5**; 357 mg, 1.11 mmol) was dissolved in *N*-methyl-2-pyrrolidone (3 mL). Thiophenol (0.11 mL, 1.11 mmol) and anhydrous  $\text{K}_2\text{CO}_3$  (184.2 mg, 1.3 mmol) were added and the solution was stirred at 150 °C for 2 h. The reaction mixture was cooled to room temperature and diluted with water. The resulting solution was acidified to pH 5 by adding 2 M HCl and the product was extracted with ethyl acetate. The organic phase was dried with  $\text{MgSO}_4$  and the solvent was removed under vacuum. The product was purified by chromatography on silica gel using ethyl acetate (100%) as eluent

to afford 207.3 mg of **7** as a yellowish solid in 61% yield.  $R_f$  ( $\text{SiO}_2$ , ethyl acetate) = 0.52, m.p. 187–190 °C. IR (KBr):  $\tilde{\nu}$  = 3382 (w), 3291 (m), 3067 (w), 2975 (w), 2934 (w), 2344 (vw), 1663 (s), 1630 (s), 1579 (s), 1541 (s), 1459 (s), 1336 (m), 1285 (s), 1196 (m), 1146 (m), 1062 (w), 936 (w), 800 (w), 769 (w), 692 (w)  $\text{cm}^{-1}$ .  $^1\text{H}$  NMR ( $\text{CD}_3\text{OD}$ , 400 MHz, 295 K):  $\delta$  = 8.45 (s, 2 H, Ar-H), 3.45 (q,  $^3J_{\text{H,H}} = 7.3$  Hz, 4 H,  $\text{CH}_2\text{-NH}$ ), 3.41 (q,  $^3J_{\text{H,H}} = 7.3$  Hz, 2 H,  $\text{CH}_2\text{-NH}$ ), 1.25 (t,  $^3J_{\text{H,H}} = 7.2$  Hz, 6 H,  $\text{CH}_3\text{-CH}_2$ ), 1.23 (t,  $^3J_{\text{H,H}} = 7.2$  Hz, 3 H,  $\text{CH}_3\text{-CH}_2$ ) ppm.  $^{13}\text{C}$  NMR ( $\text{CD}_3\text{OD}$ , 100 MHz, 295 K):  $\delta$  = 168.7 (C=O $_{ortho}$ ), 168.3 (C=O $_{para}$ ), 163.6 (C-OH), 132.8 (Ar), 126.2 (C-C=O $_{para}$ ), 119.4 (C-C=O $_{ortho}$ ), 35.9 ( $\text{CH}_2\text{-NH}$ ), 35.7 ( $\text{CH}_2\text{-NH}$ ), 14.9 ( $\text{CH}_3\text{-CH}_2$ ), 14.8 ( $\text{CH}_3\text{-CH}_2$ ) ppm. MS (ESI):  $m/z$  (%) = 330.3 (100) [M + Na] $^+$ . HRMS (ESI): calcd. for  $\text{C}_{15}\text{H}_{21}\text{N}_3\text{O}_4\text{Na}^+$  330.1424; found 330.1427 [M + Na] $^+$ .

**$N^1,N^3,N^5$ -Triethyl-2-(pent-4-ynoxy)benzene-1,3,5-tricarboxamide (9):**  $N^1,N^3,N^5$ -Triethyl-2-hydroxybenzene-1,3,5-tricarboxamide (**7**; 212 mg, 0.69 mmol) was dissolved in dry DMF (2 mL) in a vial under  $\text{N}_2$ .  $\text{Cs}_2\text{CO}_3$  (226.9 mg, 0.69 mmol) and NaI (51.7 mg, 0.35 mmol) were added and the suspension was stirred for 5 min at room temperature. 5-Chloro-1-pentyne (0.146 mL, 141.5 mg, 1.38 mmol) was added and the vial was sealed with a Teflon<sup>®</sup>-coated cap and stirred at 60 °C for 48 h. The reaction was cooled to room temperature and diluted with water. The solution was extracted with ethyl acetate and the organic phases were dried with  $\text{MgSO}_4$ . The solvent was removed under vacuum and the product was purified by chromatography on  $\text{SiO}_2$  using ethyl acetate (100%) to furnish 43 mg of **9** as a white solid in 17% yield. Suitable crystals for X-ray diffraction were obtained by slow evaporation from  $\text{CDCl}_3$ .  $R_f$  ( $\text{SiO}_2$ , ethyl acetate) = 0.15, m.p. 147–148 °C. IR (film  $\text{CDCl}_3$ ):  $\tilde{\nu}$  = 3260 (m), 3074 (w), 2974 (w), 2935 (w), 2877 (w), 1639 (s), 1539 (s), 1448 (m), 1381 (w), 1356 (w), 1297 (m), 1149 (w), 1029 (w), 665 (w)  $\text{cm}^{-1}$ .  $^1\text{H}$  NMR ( $\text{CDCl}_3$ , 400 MHz, 295 K):  $\delta$  = 8.26 (s, 2 H, Ar-H), 7.18 (t,  $^3J_{\text{H,H}} = 5.0$  Hz, 2 H,  $\text{NH}_{ortho}$ ), 6.46 (t,  $^3J_{\text{H,H}} = 4.9$  Hz, 2 H,  $\text{NH}_{para}$ ), 4.12 (t,  $^3J_{\text{H,H}} = 6.5$  Hz, 2 H, ArO- $\text{CH}_2\text{-CH}_2\text{-CH}_2$ ), 3.53–3.42 (m, 6 H,  $\text{CH}_2\text{-NH}$ ), 2.37 (dt,  $^3J_{\text{H,H}} = 6.9$ ,  $^4J_{\text{H,H}} = 2.6$  Hz, 2 H,  $\text{CH}_2\text{-CH}_2\text{-C-CH}$ ), 2.03–1.96 (m, 3 H, O- $\text{CH}_2\text{-CH}_2\text{-CH}_2$ -, Alkyne-CH), 1.26 (t,  $^3J_{\text{H,H}} = 7.3$  Hz, 6 H,  $\text{CH}_3\text{-CH}_2$ ), 1.22 (t,  $^3J_{\text{H,H}} = 7.3$  Hz, 3 H,  $\text{CH}_3\text{-CH}_2$ ) ppm.  $^{13}\text{C}$  NMR ( $\text{CDCl}_3$ , 100 MHz, 295 K):  $\delta$  = 165.5 (C=O $_{para}$ ), 164.9 (C=O $_{ortho}$ ), 156.6 (C-O), 131.9 (Ar), 131.0 (C-C=O $_{para}$ ), 129.2 (C-C=O $_{ortho}$ ), 82.6 (C-CH), 75.7 (ArO- $\text{CH}_2\text{-CH}_2\text{-CH}_2$ ), 69.8 (Alkyne-CH), 35.2 ( $\text{CH}_2\text{-NH}$ ), 35.1 ( $\text{CH}_2\text{-NH}$ ), 29.0 (ArO- $\text{CH}_2\text{-CH}_2\text{-CH}_2$ -), 15.3 (- $\text{CH}_2\text{-CH}_2\text{-C-CH}$ ), 14.89 ( $\text{CH}_3\text{-CH}_2$ ), 14.86 ( $\text{CH}_3\text{-CH}_2$ ) ppm. MS (ESI):  $m/z$  (%) = 396.5 (100) [M + Na] $^+$  769.8 (87) [2M + Na] $^+$ . HRMS (MALDI-TOF): calcd. for  $\text{C}_{20}\text{H}_{27}\text{N}_3\text{NaO}_4^+$  396.1894; found 396.1885 [M + Na] $^+$ .

**$N^1,N^3,N^5$ -Trihexyl-2-methoxybenzene-1,3,5-tricarboxamide (6):** 2-Methoxybenzene-1,3,5-tricarboxylic acid (**4**) (1.31 g, 5.46 mmol) was suspended in dry toluene (15 mL).  $\text{SOCl}_2$  (1.4 mL, 19.09 mmol) and 5 drops of DMF were added. The reaction mixture was stirred at 110 °C for 2 h. Volatile compounds were removed under high vacuum to afford a yellowish oil. The oil was dissolved in dry THF (10 mL) and added dropwise to a solution of hexylamine (5 mL, 37.8 mmol) in dry THF (10 mL) at 0 °C. The reaction mixture was stirred at 0 °C for 1 h and then for 15 h at room temperature. The organic solvent was removed under vacuum and the resulting crude solid was dissolved in ethyl acetate and washed with 2 M HCl, a 5% sol. of  $\text{NaHCO}_3$  and brine. The organic phase was dried with  $\text{MgSO}_4$  and the solvent was removed under vacuum. The product was purified by chromatography on silica gel by using ethyl acetate/toluene (1:1) to afford 1.729 g of **6** as a white amorphous solid in 64% yield.  $R_f$  ( $\text{SiO}_2$ , ethyl acetate/toluene, 1:1) = 0.36, m.p. 155.5 °C (DSC). IR ( $\text{CDCl}_3$  film):  $\tilde{\nu}$  =

3256 (m), 3076 (w), 2958 (s), 2931 (s), 2859 (m), 2245 (w), 1635 (s), 1549 (s), 1468 (m), 1423 (w), 1379 (w), 1273 (w), 1122 (vw), 1005 (w), 908 (s), 735 (s), 649 (w)  $\text{cm}^{-1}$ .  $^1\text{H}$  NMR ( $\text{CDCl}_3$ , 400 MHz, 295 K):  $\delta$  = 8.24 (s, 2 H, Ar-*H*), 7.32 (t,  $^3J_{\text{H,H}} = 5.5$  Hz, 2 H,  $\text{NH}_{ortho}$ ); 6.52 (t,  $^3J_{\text{H,H}} = 5.5$  Hz, 1 H,  $\text{NH}_{para}$ ), 3.88 (s, 3 H, OMe), 3.42 (q,  $^3J_{\text{H,H}} = 6.9$  Hz, 4 H,  $\text{CH}_2\text{-NH}$ ), 3.38 (q,  $^3J_{\text{H,H}} = 6.9$  Hz, 2 H,  $\text{CH}_2\text{-NH}$ ), 1.63–1.53 (m, 6 H,  $\text{NH-CH}_2\text{-CH}_2\text{-}$ ), 1.39–1.23 (m, 18 H, 9  $\text{CH}_2$ ), 0.90–0.85 (m, 9 H,  $\text{CH}_3$ ) ppm.  $^{13}\text{C}$  NMR ( $\text{CDCl}_3$ , 100 MHz, 295 K):  $\delta$  = 165.6 (C=O<sub>para</sub>), 164.8 (C=O<sub>ortho</sub>), 157.7 (C=O), 132.0 (Ar), 131.1 (C-C=O<sub>para</sub>), 128.7 (C-C=O<sub>ortho</sub>), 63.3 (OMe), 40.4 ( $\text{CH}_2\text{-NH}$ ), 40.2 ( $\text{CH}_2\text{-NH}$ ), 31.6 ( $\text{CH}_2$ ), 29.61 ( $\text{NH-CH}_2\text{-CH}_2\text{-}$ ), 29.56 ( $\text{NH-CH}_2\text{-CH}_2\text{-}$ ), 26.85 ( $\text{CH}_2$ ), 26.77 ( $\text{CH}_2$ ), 22.68 ( $\text{CH}_2$ ), 22.66 ( $\text{CH}_2$ ), 14.1 ( $\text{CH}_3$ ) ppm. MS (ESI):  $m/z$  (%) = 512.5 (100)  $[\text{M} + \text{Na}]^+$ . HRMS (ESI): calcd. for  $\text{C}_{28}\text{H}_{47}\text{N}_3\text{O}_4\text{Na}^+$  512.3459; found 512.3435  $[\text{M} + \text{Na}]^+$ .

**$N^1, N^3, N^5$ -Trihexyl-2-hydroxybenzene-1,3,5-tricarboxamide (8):**  $N^1, N^3, N^5$ -Trihexyl-2-methoxybenzene-1,3,5-tricarboxamide (6; 1.7 g, 3.47 mmol) was dissolved in *N*-methyl-2-pyrrolidone (8 mL). Thiophenol (0.35 mL, 3.47 mmol) and anhydrous  $\text{K}_2\text{CO}_3$  (575.8 mg, 4.16 mmol) were added and the reaction mixture was stirred at 150 °C for 2 h. It was then cooled to room temperature and diluted with water. The solution was acidified to pH 3 by adding concentrated HCl (37%). The product was extracted with dichloromethane. The organic phases were dried with  $\text{MgSO}_4$ . The solvent was removed under vacuum and the product was purified by chromatography on silica gel using cyclohexane/ethyl acetate (6:4) as eluent to afford 1.287 g of **8** as yellowish amorphous solid in 78% yield.  $R_f$  ( $\text{SiO}_2$ , cyclohexane/ethyl acetate, 6:4) = 0.49, m.p. 54 °C. IR (liquid film):  $\tilde{\nu}$  = 3306 (m), 3081 (w), 2957 (s), 2930 (s), 2858 (m), 1634 (s), 1579 (s), 1542 (s), 1464 (s), 1415 (w), 1378 (w), 1287 (m), 1194 (w), 1149 (w), 1063 (vw), 932 (w), 806 (w), 768 (w), 727 (w), 674 (w)  $\text{cm}^{-1}$ .  $^1\text{H}$  NMR ( $\text{CDCl}_3$ , 400 MHz, 295 K):  $\delta$  = 8.57 (s, 2 H, Ar-*H*), 7.88 (br., 2 H,  $\text{NH}_{ortho}$ ), 6.61 (t,  $^3J_{\text{H,H}} = 5.2$  Hz, 1 H,  $\text{NH}_{para}$ ), 3.47–3.37 (m, 6 H,  $\text{CH}_2\text{-NH}$ ), 1.63–1.52 (m, 6 H,  $\text{NH-CH}_2\text{-CH}_2\text{-}$ ), 1.37–1.26 (m, 18 H, 9  $\text{CH}_2$ ), 0.90–0.85 (m, 9 H,  $\text{CH}_3$ ) ppm.  $^{13}\text{C}$  NMR ( $\text{CDCl}_3$ , 100 MHz, 295 K)\*:  $\delta$  = 166.6 (C=O<sub>para</sub>), 163.2 (C=O<sub>ortho</sub>), 131.9 (C-C=O<sub>para</sub> C-C=O<sub>ortho</sub>)\*\*, 124.7 (Ar), 40.5 ( $\text{CH}_2\text{-NH}$ ), 40.1 ( $\text{CH}_2\text{-NH}$ ), 31.61 ( $\text{CH}_2$ ), 31.58 ( $\text{CH}_2$ ), 29.6 ( $\text{NH-CH}_2\text{-CH}_2\text{-}$ ), 29.3 ( $\text{NH-CH}_2\text{-CH}_2\text{-}$ ), 26.81 ( $\text{CH}_2$ ), 26.79 ( $\text{CH}_2$ ), 22.6 ( $\text{CH}_2$ ), 14.1 ( $\text{CH}_3$ ) ppm. MS (ESI):  $m/z$  (%) = 499.0 (100)  $[\text{M} + \text{Na}]^+$ . HRMS (ESI): calcd. for  $\text{C}_{27}\text{H}_{45}\text{N}_3\text{O}_4\text{Na}^+$  498.3302; found 498.3300  $[\text{M} + \text{Na}]^+$ . \* C-O aromatic signal was not detected. \*\* Very broad signal.

**$N^1, N^3, N^5$ -Trihexyl-2-(pent-4-ynyloxy)benzene-1,3,5-tricarboxamide (2):**  $N^1, N^3, N^5$ -Trihexyl-2-hydroxybenzene-1,3,5-tricarboxamide (**8**; 610 mg, 1.28 mmol) was dissolved in dry DMF (2 mL) in a vial. KI (212 mg, 1.28 mmol) and anhydrous  $\text{Cs}_2\text{CO}_3$  (424 mg, 1.28 mmol) were added and the suspension was stirred for 5 min at room temperature. 5-Chloro-1-pentyne (0.41 mL, 3.85 mmol) was then added and the vial was sealed with a Teflon<sup>®</sup>-coated cap and stirred at 70 °C for 48 h and for another 48 h at room temperature. The reaction was diluted in water and the solution was extracted with ethyl acetate. The organic phases were dried with  $\text{MgSO}_4$  and the solvent was removed under vacuum. The product was purified by chromatography on silica gel using cyclohexane/ethyl acetate (6:4) as eluent to furnish 292 mg of **2** as colourless solid in 42% yield.  $R_f$  ( $\text{SiO}_2$ , cyclohexane/ethyl acetate, 6:4) = 0.46, m.p. 141.1 °C (see Table 1). IR (KBr):  $\tilde{\nu}$  = 3246 (m), 3079 (w), 2930 (m), 2859 (m), 1634 (s), 1552 (s), 1451 (m), 1376 (w), 1297 (m), 1033 (w), 915 (w), 725 (w)  $\text{cm}^{-1}$ .  $^1\text{H}$  NMR ( $\text{CDCl}_3$ , 400 MHz, 295 K):  $\delta$  = 8.25 (s, 2 H, Ar-*H*), 7.17 (t,  $^3J_{\text{H,H}} = 5.6$  Hz, 2 H,  $\text{NH}_{ortho}$ ), 6.44 (t,  $^3J_{\text{H,H}} = 5.6$  Hz, 2 H,  $\text{NH}_{para}$ ), 4.11 (t,  $^3J_{\text{H,H}} = 6.5$  Hz, 2 H, O- $\text{CH}_2\text{-CH}_2\text{-CH}_2\text{-}$ ), 3.46–3.37 (m, 6 H,  $\text{CH}_2\text{-NH}$ ), 2.35 (dt,  $^3J_{\text{H,H}} = 6.9$ ,  $^4J_{\text{H,H}}$

= 2.6 Hz, 2 H,  $\text{CH}_2\text{-CH}_2\text{-C-CH}$ ), 2.01–1.93 (m, 3 H, O- $\text{CH}_2\text{-CH}_2\text{-CH}_2\text{-}$ , Alkyne-*CH*), 1.63–1.53 (m, 6 H,  $\text{NH-CH}_2\text{-CH}_2\text{-}$ ), 1.41–1.27 (m, 18 H, 3  $\times$  6  $\text{CH}_2$ ), 0.90–0.85 (m, 9 H,  $\text{CH}_3$ ) ppm.  $^{13}\text{C}$  NMR ( $\text{CDCl}_3$ , 100 MHz, 295 K):  $\delta$  = 165.5 (C=O<sub>para</sub>), 165.0 (C=O<sub>ortho</sub>), 156.5 (C-O), 131.8 (Ar), 131.0 (C-C=O<sub>para</sub>), 129.2 (C-C=O<sub>ortho</sub>), 82.6 (C-CH), 75.7 (O- $\text{CH}_2\text{-CH}_2\text{-CH}_2\text{-}$ ), 69.7 (Alkyne-*CH*), 40.4 ( $\text{CH}_2\text{-NH}$ ), 40.3 ( $\text{CH}_2\text{-NH}$ ), 31.6 ( $\text{CH}_2$ ), 29.7 ( $\text{NH-CH}_2\text{-CH}_2\text{-}$ ), 28.9 (O- $\text{CH}_2\text{-CH}_2\text{-CH}_2\text{-}$ ), 26.9 ( $\text{CH}_2$ ), 26.8 ( $\text{CH}_2$ ), 22.68 ( $\text{CH}_2$ ), 22.67 ( $\text{CH}_2$ ), 15.3 (- $\text{CH}_2\text{-CH}_2\text{-C-CH}$ ), 14.1 ( $\text{CH}_3\text{-CH}_2\text{-}$ ) ppm. MS (ESI):  $m/z$  (%) = 564.6 (100)  $[\text{M} + \text{Na}]^+$ . HRMS (MALDI-TOF): calcd. for  $\text{C}_{32}\text{H}_{51}\text{N}_3\text{NaO}_4^+$  564.3772; found 564.3773  $[\text{M} + \text{Na}]^+$ .

**2-Bromobenzene-1,3,5-tricarboxylic Acid (10):** Compound **10** was synthesized according to the procedure reported by Wallenfels et al.<sup>[29]</sup> 2-Bromomesitylene (2.6 g, 13.07 mmol) was dissolved in a mixture of *tert*-butyl alcohol (150 mL) and distilled water (350 mL).  $\text{K}_2\text{CO}_3$  (5.42 g, 39.21 mmol) was added and the solution was stirred for 5 min.  $\text{KMnO}_4$  (20.65 g, 130.7 mmol) was slowly added and the dark-violet solution was stirred at 100 °C for 9 h. The reaction mixture was then cooled to room temperature and the excess permanganate was reduced by slowly adding solid  $\text{Na}_2\text{S}_2\text{O}_3$ . The brown solid was filtered off and *tert*-butyl alcohol was removed by distillation under rotatory evaporation. The aqueous solution was acidified with concentrated HCl (37%) until pH 3, saturated with solid NaCl and extracted with ethyl acetate. The organic phases were dried with  $\text{MgSO}_4$  and the solvent was removed under vacuum. The white solid obtained was washed with dichloromethane to afford 2.3 g of **10** as a white solid in 62% yield. The crude product was used without further purifications, m.p. 275–276 °C. IR (solid KBr):  $\tilde{\nu}$  = 3075 (m), 1699 (s), 1385 (w), 1284 (w), 1241 (m), 1033 (w), 922 (w), 763 (w), 674 (w)  $\text{cm}^{-1}$ .  $^1\text{H}$  NMR (DMSO, 400 MHz, 295 K):  $\delta$  = 8.15 (s, 2 H, Ar-*H*) ppm.  $^{13}\text{C}$  NMR (DMSO, 100 MHz, 295 K):  $\delta$  = 167.0 (C=O<sub>ortho</sub>), 165.4 (C=O<sub>para</sub>), 137.1 (C-Br), 131.0 (Ar), 130.3 (C-C=O<sub>ortho</sub>), 121.6 (C-C=O<sub>para</sub>) ppm.

**2-Bromo- $N^1, N^3, N^5$ -trihexylbenzene-1,3,5-tricarboxamide (3):** 2-Bromobenzene-1,3,5-tricarboxylic acid (**10**; 80 mg, 0.277 mmol) was dissolved in dry DMF (3 mL) and cooled to 0 °C under nitrogen. EDC-HCl (191.2 mg, 0.997 mmol) and *N*-hydroxysuccinimide (127.5 mg, 1.108 mmol) were added and the murky solution was stirred at 0 °C for 5 min. A solution of hexylamine (0.128 mL, 0.969 mmol) dissolved in dry DMF (2 mL) was slowly added to the reaction at 0 °C. The reaction was stirred for 15 min at 0 °C and then at 45 °C for 18 h. The reaction mixture was diluted with ethyl acetate (15 mL) and the organic phase was washed with 2 M HCl (2  $\times$  15 mL), 10%  $\text{Na}_2\text{CO}_3$  (2  $\times$  10 mL) and brine (1  $\times$  15 mL). The organic phase was dried with  $\text{MgSO}_4$  and the solvent was removed under reduced pressure. The product was purified by chromatography on silica gel using toluene/ethyl acetate (4:6) as eluent to afford 27 mg of **3** as a white solid in 18% yield.  $R_f$  ( $\text{SiO}_2$ , toluene/AcOEt, 4:6) = 0.42, m.p. 239.5 °C (see Table 1). IR (KBr):  $\tilde{\nu}$  = 3271 (m), 3081 (w), 2957 (m), 2929 (m), 2857 (m), 1639 (s), 1553 (s), 1467 (m), 1378 (w), 1304 (w), 1149 (w), 1028 (w), 908 (w), 726 (w)  $\text{cm}^{-1}$ .  $^1\text{H}$  NMR ( $\text{CDCl}_3$ , 400 MHz, 295 K,  $c = 20$  mm)\*:  $\delta$  = 8.06 (s, 1 H,  $\text{NH}_{para}$ ), 7.71 (s, 2 H,  $\text{NH}_{ortho}$ ), 7.12 (s, 2 H, Ar-*H*), 3.32–3.29 (m, 6 H,  $\text{CH}_2\text{-NH}$ ), 1.63–1.56 (m, 6 H,  $\text{NH-CH}_2\text{-CH}_2\text{-}$ ), 1.36–1.25 (m, 18 H, 3  $\times$  6  $\text{CH}_2$ ), 0.93–0.88 (m, 9 H,  $\text{CH}_3$ ) ppm.  $^{13}\text{C}$  NMR ( $\text{CDCl}_3$ , 100 MHz, 295 K,  $c = 20$  mm)\*\*:  $\delta$  = 167.3 (C=O), 138.5 (C-Br), 127.9 (Ar), 40.6 ( $\text{CH}_2\text{-NH}$ ), 40.3 ( $\text{CH}_2\text{-NH}$ ), 31.7 ( $\text{CH}_2$ ), 29.3 ( $\text{NH-CH}_2\text{-CH}_2\text{-}$ ), 27.0 ( $\text{CH}_2$ ), 26.9 ( $\text{CH}_2$ ), 22.8 ( $\text{CH}_2$ ), 14.2 ( $\text{CH}_3$ ) ppm. MS (ESI):  $m/z$  (%) = 560.7 (100)  $[\text{M} + \text{Na}]^+$ , 562.6 (100)  $[\text{M} + \text{Na}]^+$ . HRMS (MALDI-TOF): calcd. for  $\text{C}_{27}\text{H}_{45}\text{BrN}_3\text{O}_3^+$  538.2639 and 540.2618; found 538.2643  $[\text{M} + \text{H}]^+$  and 540.2611  $[\text{M} + \text{H}]^+$ . \* All the signals are broad due to intense

association of the solute. \*\* Two aromatic signals ( $C-C=O_{ortho}$  and  $C-C=O_{para}$ ) were not detected.

**Crystallographic Information:** CCDC-1055357 (for **9**) contains the supplementary crystallographic data for this paper. These data can be obtained free of charge from The Cambridge Crystallographic Data Centre via [www.ccdc.cam.ac.uk/data\\_request/cif](http://www.ccdc.cam.ac.uk/data_request/cif).

Further details of the single-crystal X-ray diffraction study are provided in the Supporting Information.

## Acknowledgments

The authors thank Dr. Armelle Vallat-Michel and Mr. Fredy Nydegger (NPAC University of Neuchâtel) for her assistance with the mass spectrometry and Dr. Sebastiano Guerra and Prof. Deschenaux (UniNE) for POM and DSC analyses. Financial support by the University of Neuchâtel and the Swiss National Science Foundation (grant number 200020-140555) are gratefully acknowledged.

- [1] G. M. Whitesides, M. Boncheva, *Proc. Natl. Acad. Sci. USA* **2002**, *99*, 4769–4774.
- [2] S. I. Stupp, L. C. Palmer, *Chem. Mater.* **2014**, *26*, 507–518.
- [3] Y. Matsunaga, N. Miyajima, Y. Nakayasu, S. Sakai, M. Yonenaga, *Bull. Chem. Soc. Jpn.* **1988**, *61*, 207–210.
- [4] a) P. Besenius, J. L. M. Heynens, R. Straathof, M. M. L. Nieuwenhuizen, P. H. H. Bomans, E. Terreno, S. Aime, G. J. Strijkers, K. Nicolay, E. W. Meijer, *Contrast Media Mol. Imaging* **2012**, *7*, 356–361; b) S. Cantekin, T. F. A. de Greef, A. R. A. Palmans, *Chem. Soc. Rev.* **2012**, *41*, 6125–6137; c) T. Shikata, D. Ogata, K. Hanabusa, *J. Phys. Chem. B* **2004**, *108*, 508–514.
- [5] C. A. Hunter, J. K. M. Sanders, *J. Am. Chem. Soc.* **1990**, *112*, 5525–5534.
- [6] L. Brunsveld, H. Zhang, M. Glasbeek, J. A. J. M. Vekemans, E. W. Meijer, *J. Am. Chem. Soc.* **2000**, *122*, 6175–6182.
- [7] a) M. P. Lightfoot, F. S. Mair, R. G. Pritchard, J. E. Warren, *Chem. Commun.* **1999**, 1945–1946; b) P. J. M. Stals, M. M. J. Smulders, R. Martin-Rapun, A. R. A. Palmans, E. W. Meijer, *Chem. Eur. J.* **2009**, *15*, 2071–2080.
- [8] a) M. L. Bushey, A. Hwang, P. W. Stephens, C. Nuckolls, *J. Am. Chem. Soc.* **2001**, *123*, 8157–8158; b) M. L. Bushey, T.-Q. Nguyen, C. Nuckolls, *J. Am. Chem. Soc.* **2003**, *125*, 8264–8269; c) M. L. Bushey, T.-Q. Nguyen, W. Zhang, D. Horoszewski, C. Nuckolls, *Angew. Chem. Int. Ed.* **2004**, *43*, 5446–5453; *Angew. Chem.* **2004**, *116*, 5562.
- [9] a) D. Thevenet, Ph.D. thesis no. 2182, University of Neuchâtel, **2010**; <http://doc.rero.ch/record/21252?ln=fr>; b) D. Thevenet, R. Neier, *Synthesis* **2011**, 3801–3806.
- [10] L. Schmidt-Mende, A. Fechtenkötter, K. Mullen, E. Moons, R. H. Friend, J. D. MacKenzie, *Science* **2001**, *293*, 1119–1122.
- [11] S. Kumar, *Liq. Cryst.* **2005**, *32*, 1089–1113.
- [12] T. Curtius, *J. Prakt. Chem.* **1915**, *91*, 39–102.
- [13] a) M. M. J. Smulders, M. M. L. Nieuwenhuizen, T. F. A. de Greef, P. van der Schoot, A. P. H. J. Schenning, E. W. Meijer, *Chem. Eur. J.* **2010**, *16*, 362–367; b) M. M. J. Smulders, A. P. H. J. Schenning, E. W. Meijer, *J. Am. Chem. Soc.* **2008**, *130*, 606–611; c) T. F. A. De Greef, M. M. J. Smulders, M. Wolffs, A. P. H. J. Schenning, R. P. Sijbesma, E. W. Meijer, *Chem. Rev.* **2009**, *109*, 5687–5754; d) A. J. Markvoort, H. M. M. ten Eikelder, P. A. J. Hilbers, T. F. A. de Greef, E. W. Meijer, *Nat. Commun.* **2011**, *2*, 1517/1511–1517/1519.
- [14] A. R. A. Palmans, J. A. J. M. Vekemans, E. E. Havinga, E. W. Meijer, *Angew. Chem. Int. Ed. Engl.* **1997**, *36*, 2648–2651; *Angew. Chem.* **1997**, *109*, 2763.
- [15] A. R. A. Palmans, J. A. J. M. Vekemans, H. Fischer, R. A. Hikmet, E. W. Meijer, *Chem. Eur. J.* **1997**, *3*, 300–307.
- [16] T.-Q. Nguyen, M. L. Bushey, L. E. Brus, C. Nuckolls, *J. Am. Chem. Soc.* **2002**, *124*, 15051–15054.
- [17] T.-Q. Nguyen, R. Martel, P. Avouris, M. L. Bushey, L. Brus, C. Nuckolls, *J. Am. Chem. Soc.* **2004**, *126*, 5234–5242.
- [18] a) L. Fielding, *Tetrahedron* **2000**, *56*, 6151–6170; b) R. S. Macomber, *J. Chem. Educ.* **1992**, *69*, 375–378; c) P. Thordarson, *Chem. Soc. Rev.* **2011**, *40*, 1305–1323.
- [19] R. B. Martin, *Chem. Rev.* **1996**, *96*, 3043–3064.
- [20] a) C. S. Johnson Jr., *Prog. Nucl. Magn. Reson. Spectrosc.* **1999**, *34*, 203–256; b) A. Macchioni, G. Ciancaleoni, C. Zuccaccia, D. Zuccaccia, *Chem. Soc. Rev.* **2008**, *37*, 479–489; c) K. F. Morris, P. Stilbs, C. S. Johnson Jr., *Anal. Chem.* **1994**, *66*, 211–215.
- [21] a) L. Allouche, A. Marquis, J.-M. Lehn, *Chem. Eur. J.* **2006**, *12*, 7520–7525; b) A. Perez, D. de Saa, A. Ballesteros, J. L. Serano, T. Sierra, P. Romero, *Chem. Eur. J.* **2013**, *19*, 10271–10279.
- [22] a) I. B. Rietveld, D. Bedeaux, *Macromolecules* **2000**, *33*, 7912–7917; b) A. Sagidullin, B. Fritzingler, U. Scheler, V. D. Skirda, *Polymer* **2004**, *45*, 165–170.
- [23] W. S. Price, F. Tsuchiya, Y. Arata, *J. Am. Chem. Soc.* **1999**, *121*, 11503–11512.
- [24] H. C. Kolb, M. G. Finn, K. B. Sharpless, *Angew. Chem. Int. Ed.* **2001**, *40*, 2004–2021; *Angew. Chem.* **2001**, *113*, 2056.
- [25] G.-L. Law, T. A. Pham, J. Xu, K. N. Raymond, *Angew. Chem. Int. Ed.* **2012**, *51*, 2371–2374.
- [26] A. K. Chakraborti, L. Sharma, M. K. Nayak, *J. Org. Chem.* **2002**, *67*, 6406–6414.
- [27] a) D. Kanamori, A. Furukawa, T.-A. Okamura, H. Yamamoto, N. Ueyama, *Org. Biomol. Chem.* **2005**, *3*, 1453–1459; b) D. Kanamori, T.-a. Okamura, H. Yamamoto, S. Shimizu, Y. Tsujimoto, N. Ueyama, *Bull. Chem. Soc. Jpn.* **2004**, *77*, 2057–2064; c) D. Kanamori, T.-a. Okamura, H. Yamamoto, N. Ueyama, *Angew. Chem. Int. Ed.* **2005**, *44*, 969–972; *Angew. Chem.* **2005**, *117*, 991.
- [28] K. Wallenfels, K. Friedrich, F. Witzler, *Tetrahedron* **1967**, *23*, 1353–1358.
- [29] X. Hou, M. Schober, Q. Chu, *Cryst. Growth Des.* **2012**, *12*, 5159–5163.
- [30] M. M. L. Nieuwenhuizen, T. F. A. de Greef, R. L. J. van der Bruggen, J. M. J. Paulusse, W. P. J. Appel, M. M. J. Smulders, R. P. Sijbesma, E. W. Meijer, *Chem. Eur. J.* **2010**, *16*, 1601–1612.
- [31] D. Wu, A. Chen, C. S. Johnson Jr., *J. Magn. Reson., Ser. A* **1995**, *115*, 260–264.
- [32] *OriginPro 8, Data Analysis and Graphing Software*, OriginLab Cooperation, Northampton, MA 01060, USA.
- [33] *Perkin-Elmer Spectrum™ 5, Infrared Spectroscopy Software Platform*, Perkin-Elmer, Waltham, MA 02451, USA.

Received: April 21, 2015

Published Online: July 14, 2015